LENGTH-DEPENDENT SELECTIVE KILLING OF BRAIN CANCER CELLS USING POLYGUANINE-MODIFIED GOLD NANOPARTICLES

by
Gizem Uçankuş

Submitted to Graduate School of Natural and Applied Sciences
in Partial Fulfillment of the Requirements
for the Degree of Master of Science in
Biotechnology

Yeditepe University
2017

LENGTH-DEPENDENT SELECTIVE KILLING OF BRAIN CANCER CELLS USING POLYGUANINE-MODIFIED GOLD NANOPARTICLES

APPROVED BY:

Prof. Dr. Mustafa Çulha
(Thesis Supervisor) .....

Prof. Dr. Bahattin Yalçın .....

Assist. Prof. Dr. Hüseyin Çimen .....

DATE OF APPROVAL: ..../..../2017

ACKNOWLEDGEMENTS

First, I would like to express my gratitude to my supervisor Prof. Dr. Mustafa Çulha for his guidance throughout my master period. His guidance has inspired me and working with him has been a great opportunity.

I am thankful to Prof. Dr. Fikrettin Şahin and Assist. Prof. Dr. Hüseyin Çimen for their permission to use their laboratory facilities.

Moreover, I would like to thank all my colleagues from Yeditepe University Nanotechnology Research Group, especially, Pınar Akkuş, Mine Altunbek, Deniz Yaşar Öztaş and Deniz Uzunoğlu for inspiring me with their advices and knowledge. They have always encouraged me to improve myself. I would also like to thank Firdevs Cansu Atılgan, Eray Esendir and İnci Kurt for their valuable support and motivation.

Most importantly, I would like to express my deepest appreciation to my family and my friends for their endless support, encouragement and patience, and for always being there.

ABSTRACT

LENGTH-DEPENDENT SELECTIVE KILLING OF BRAIN CANCER CELLS USING POLYGUANINE MODIFIED GOLD NANOPARTICLES

Gold nanoparticles (AuNPs) are investigated as a promising therapeutic agent in nanomedicine due to their easy synthesis and surface functionalization. AuNPs also have extraordinary physicochemical properties such as inertness, being plasmonic and biocompatible. AuNPs can be modified using variety of molecules including biological ones, such as deoxyribonucleic acid (DNA), peptides, proteins, carbohydrates for highly exciting applications in various fields of therapeutic nanomedicine such as drug delivery, gene therapy, sensing, detection, and imaging. Among these biological molecules, therapeutic use of oligonucleotides, more specifically guanine-rich (G-rich) oligonucleotides, gain interest due to their anti-proliferative effects in malignant tumor cells. Surface functionalization of AuNPs using G-rich oligonucleotides are being studied in nanomedicine, however, little is known about the cellular response of these hybrid structures as potential therapeutic agents. In this study, we aimed to investigate length-dependent cellular responses of oligonucleotide modified-AuNPs. With this goal in mind, polyadenine-tailed polyguanine sequences (G10 and G20) are used to functionalize the surface of AuNPs. Resulting nanostructures, G10-AuNPs and G20-AuNPs, are used to investigate their effect through cell cycle analysis, apoptosis induction, cellular uptake studies, as well as *in vitro* cytotoxicity assessments. As a result, increasing number of guanine bases showed enhanced cellular uptake (1.86 fold), increased cell accumulation in S phase (1.67-fold) and G_2/M phase (1.34-fold), and elevated induction of apoptosis (two-fold) in glioblastoma (GBM) cells (U87MG and U373) when compared with normal human astrocytes (NHA). In conclusion, the data suggests length-dependent selective killing of GBM cells using polyguanine modified-AuNPs.

ÖZET

POLİGUANİN-MODİFİYE ALTIN NANOPARÇACIKLAR İLE BEYİN KANSERİ HÜCRELERİNİN UZUNLUK-BAĞIMLI SEÇİÇİ ÖLÜMÜ

Sentezi ve yüzey modifikasyon reaksiyonları kolay olması sebebiyle altın nanoparçacıklar (AuNP) nanotıp alanında gelecek vaadeden bir terapötik ajan olarak çalışılmaktadır. Aynı zamanda, AuNP'ler, inert, biyouyumlu ve plazmonik olma özelliklerinden kaynaklı olağanüstü fiziksel ve kimyasal özelliklere sahip nanoparçacıklardır. AuNP'lerin yüzeyleri deoksiribonükleik asit (DNA), peptit, protein, karbonhidrat gibi birçok farklı biyolojik molekülerle modifiye edilebilir ve yüzeyleri modifiye olmuş AuNP'ler ilaç taşıma, gen terapisi, algılama, tespit ve görüntüleme gibi terapötik nanotıp alanlarında oldukça merak uyandırıcıdırlar. Bu biyomoleküller arasında guanince-zengin (G-zengin) oligonükleotitlerin terapötik kullanımları oldukça ilgi çekmektedir çünkü kanser hücreleri üzerinde anti-proliferatif özellikleri vardır. G-zengin oligonükleotitle yüzey modifiye AuNP'ler çalışılmakla birlikte, bu potansiyel terapötik taşıyıcıların hücresel tepkileri hakkında az bilgi bilinmektedir. Bu çalışmada, oligonükleotit-modifiye AuNP'lerin uzunluk-bağımlı hücresel tepkilerinin araştırılması amaçlanmıştır. Bu çerçevede, AuNP yüzey modifikasyonları için poliadenin kuyruklu poliguanin (G10 ve G20) sekansları kullanılmıştır. Elde edilen nanoparçacıklar, G10-AuNP ve G20-AuNP, hücre döngüsü analizi, apoptoz indüksiyonu, hücre içeri alım çalışmaları, ve bunlara ek olarak *in vitro* sitotoksisite testlerinde kullanılmıştır. Artan guanin bazı uzunluğunun glioblastom (GBM) hücrelerinde normal hücrelere kıyasla hücre içine alımını artırdığı (1.86 kat), S fazında (1.67 kat) ve G_2/M (1.34 kat) fazında hücre birikimini fazlalaştırdığı ve apoptoz indüksiyonunu artırdığı (iki kat) bulunmuştur. Sonuç olarak, elde edilen datalar poliguanin-modifiye AuNP'lerin GBM hücrelerinde uzunluk-bağımlı seçici ölüme yol açtığını göstermektedir.

TABLE OF CONTENTS

LIST OF FIGURES

LIST OF TABLES

LIST OF SYMBOLS/ABBREVIATIONS

182-SNAs	miR-182 functionalized AuNPs
Å	Ångström
AFM	Atomic force microscopy
ALT	Alternative lengthening of telomere
AuNPs	Gold nanoparticles
BBB	Blood brain barrier
BTB	Blood tumor barrier
CdSe	Cadmium selenide
CNS	Central nervous system
COOH	The carboxyl group
DLS	Dynamic light scattering
DMEM	Dulbecco's modified Eagle medium
DMSO	Dimethyl sulfoxide
DNA	Deexyribonucleic acid
Oligo-AuNPs	Oligonucleotide-modified gold nanoparticles
DOX	Doxorubicin
EDTA	Ethylenediaminetetraacetic acid
EPR	Enhanced permeability and retention
FBS	Fetal bovine serum
FT-IR	Fourier transmission infrared
G-rich	Guanine-rich
GBM	Glioblastoma
HIF2A	Hypoxia-inducible factor 2α
LSPR	Localized surface plasmon resonance
miRNA	Micro RNA
mg	Milligram
ml	Milliliter
mM	Millimolar
M	Molar
nm	Nanometer

nM	Nanomolar
nmol	Nanomole
NH_2	The amino group
NHA	Normal human astrocytes
NMR	Nuclear magnetic resonance
OD	Optical density
PBS	Phosphate buffered saline
PI	Propidium Iodide
PTT	Photothermal therapy
QDs	Quantum dots
RES	Reticuloendothelial system
RT	Room temperature
RNA	Ribonucleic acid
RGD	Arginine-glycine-aspartic acid
SDS	Sodium dodecyl sulfate
siL12-SNAs	*Bcl2L12*-specific SNAs
siRNA	Small interfering RNA
SH	The thiol group
shRNA	Short hairpin RNA
SNAs	Spherical nucleic acids
SR-A	Scavenger receptor-A
SPR	Surface plasmon resonance
TEM	Transmission electron microscoy
TMZ	Temozolomide
VEGFR	Vascular endothelial growth factor receptor
WHO	World health organization
µl	Microliter
ζ-potential	Zeta potential

1. INTRODUCTION

1.1. GOLD NANOPARTICLES

Gold nanoparticles (AuNPs) are transition metal nanoparticles, which are widely used for therapeutic, imaging and diagnostic purposes due to their several unique properties including being plasmonic, easy surface chemistry and biocompatibility. Synthesis of pure gold colloid was first described in 1857 by Michael Faraday [1], and only after 100 years later, in 1951, first structural studies of AuNPs were performed by Turkevich *et al*. [2]. Later, the method for AuNPs synthesis was developed by Frens G. in 1973 [3]. In this method, AuNPs of average diameter ranging from 160 Å to 1500 Å (1 ångström is equal to 0.1 nm) are produced by the reduction of gold salts in sodium citrate solution, in which citrate is used as both reducing and stabilizing agent. The desired size of AuNPs in colloidal suspension can be synthesized by modifying the concentration of sodium citrate solution, which is added in nucleation step. According to this method, the monodisperse 13 nm AuNPs can be synthesized by adjusting the sodium citrate solution amount to 10 per cent of the total volume of the gold chloride solution.

AuNPs in colloidal suspension exhibit unique physical, optical and chemical properties due to being biologically inert and biocompatible. The synthesized AuNPs are mostly monodisperse in suspension, and have tunable size and shape [4]. Moreover, AuNPs have strong optical properties due to LSPR (localized surface plasmon resonance) of AuNPs, resulting from the interaction of electron system of the particle with incident light [5], in visible region of electromagnetic spectrum (390-750 nm wavelength), which provide a suitable platform for biological and biomedical applications of AuNPs in nanomedicine [6, 7].

First, in 1979, Butten and Hopkins used AuNPs as probes for electron microscopy, and these probes are used in immunohistochemistry techniques [8]. Then, in 2003, a research group in Rice University, O'Neal and his co-workers, developed gold nanoshells (130 nm) used for non-invasive breast cancer diagnosis and treatment due to their near-infrared light absorption property when tuned in size [9]. AuNPs have a great potential to be a powerful tool in nanomedicine, they can be used as drug carriers (10-100 nm) providing targeted

delivery of drugs by targeting specific tumor markers, ligands and surface receptors, also by increasing the drug solubility, and improving its half-life while reducing side-effect [10, 11]. Moreover, AuNPs are suitable for their combinations with various electromagnetic sources provided by ultrasound, microwaves or laser light to perform photothermal therapies (PTT) [9, 12, 13], as well as with conventional ones; radiotherapy or chemotherapy [14, 15].

1.1.1. Size, Shape and Surface Chemistry of Gold Nanoparticles

The surface of AuNPs can be modified easily using various biological molecules such as deoxyribonucleic acid (DNA), peptides, proteins and enzymes, carbohydrates, and lipids for wide range of biomedical applications since the surface of gold metal has strong affinity for several functional groups such as thiol group (–SH), amino group ($–NH_2$), and carboxyl group (–COOH). However, (–SH) provides the strongest affinity for gold surfaces, and Au-S bond is established on the surface. Easy surface modification of AuNPs make them intriguing agents in diagnostics, sensing, cellular labeling, and also increase their use for therapeutic applications such as gene and drug delivery. Engineered AuNPs can be obtained in different sizes and shapes, as well as different surface chemistries, which alter their cellular responses such as their cellular internalization, uptake mechanism, cellular toxicity and apoptosis.

The cellular internalization of AuNPs, which had an average size of ~50 nm, was mainly achieved by clathrin-mediated endocytosis [16]. Internalized AuNPs accumulated in lysosomes, in where AuNPs were trapped and alkalize the lysosome, which would restrict its autophagy process [17, 18]. Size of AuNPs affected its distribution inside of the cell. Oh et al. demonstrated that 2.4 nm AuNPs entered nucleus, and larger ones, 5.5 nm and 8.2 nm AuNPs were located outside of the nucleus [19]. In addition, Huang et al. found that 2 nm and 6 nm AuNPs deeply penetrated into tissues, as well as entered nucleus, while 15 nm AuNPs only accumulated in cytoplasm [20]. Size of AuNPs also affects its endocytosis rate and amount. The smaller AuNPs (10-50 nm) entered and removed faster than the larger AuNPs (74-250 nm) [16, 21]. Based on this, the size of the AuNPs should be chosen according to its purpose, and also depending on cell type because size also affects the binding ligand density on AuNPs' surface; hence, the cellular uptake, the distribution

inside of the cell and cellular responses can be altered when engineered AuNPs are used [22, 23].

AuNPs can be synthesized in various shapes. However, the most popular ones are nanospheres [24, 25], nanorods [26, 27], nanocages [28, 29], nanoshells [30], nanostars [31, 32], and nanoflowers [12, 33]. In Figure 1.1, transmission electron microscopy (TEM) images of Au nanostructures in various shapes and sized are seen [12]. Among all shapes, the most preferred ones are monodispersed Au nanorods and nanospheres because the monodispersity is crucial for their use as therapeutic or diagnostic agents, and surface functionalization of nanospheres and nanorods is easier than the others. Chithrani et al. investigated alterations in cellular uptake of protein-coated AuNP, and demonstrated that both size and shape affected the cellular uptake and removal of these engineered AuNPs [16, 22]. Shape could alter the cellular internalization due to changed contact area of AuNPs. Rod-shaped AuNPs have greater surface contact area than sphere-shaped ones, which in turn reduces the number of interacted surface receptors. In addition, when shape of the AuNP is not spherical, the surface coating is also not obtained homogenous, which also weakens the binding of rod-shaped AuNPs on the surface of cells and so reduces the cellular uptake [22].

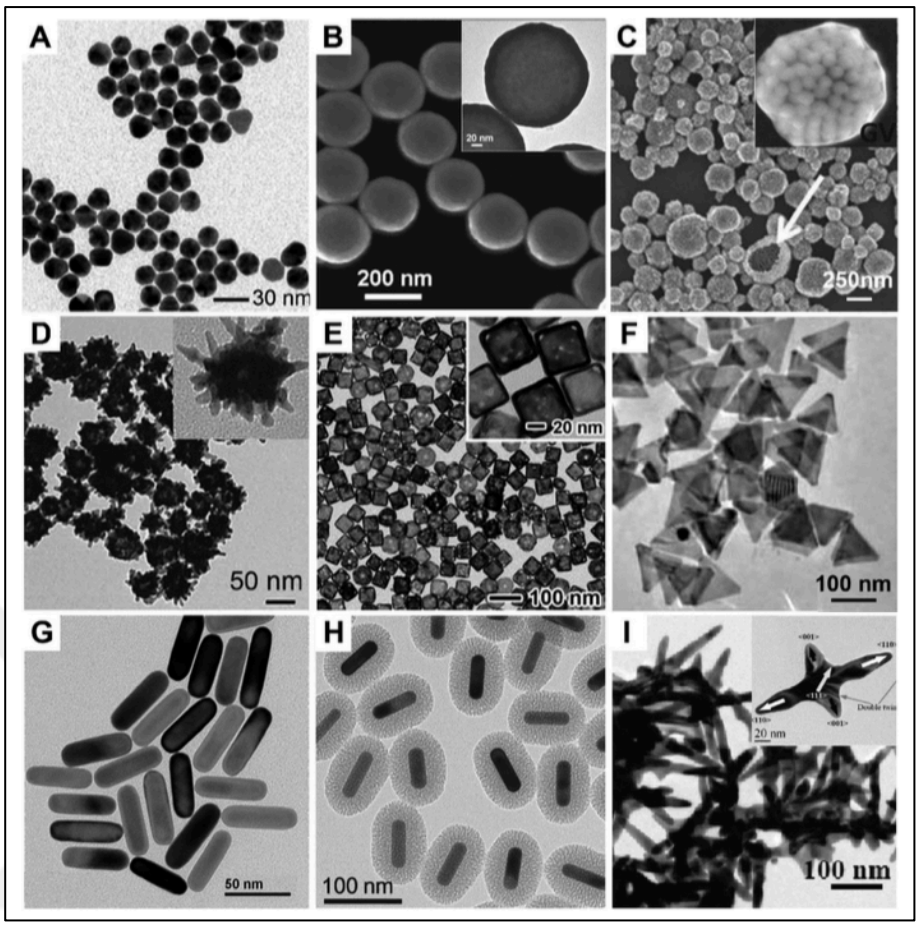

Figure 1.1. TEM images of AuNPs with different sizes and shapes. (A) Au nanospheres [34], (B) Au nanoshells [35], (C) Au nanovesicles [36], (D) Au nanostars [34], (E) Au nanocages [37], (F) Au nanoprisms [38], (G) Au nanorods [39], (H) Silica-coated Au nanorods [40], and (I) Au nanocrosses [41].

Surface chemistry also changes the cellular internalization and other cellular responses due to increased amount of uptake of surface functionalized-AuNPs by cells. Modification of the surface of AuNPs with certain proteins, amino-acid sequences, and oligonucleotides affects cellular internalization. Jiang et al. demonstrated that 40-50 nm Herceptin-coated AuNPs increased apoptosis induction by activating caspase enzymes [42]. Moreover, peptide modifications can be used for targeting purposes because they have strong binding affinities for specific surface receptors. Integrins are one of the surface receptors used for tumor targeting, Arginine-Glycine-Aspartic acid (RGD) modified-AuNPs increased cellular uptake and efficiently used in gene delivery and PTT in several studies [43-45]. RGD-based peptides achieve increased cellular uptake due to their selective cell membrane penetrating capacity. Targeting delivery is not only achieved by surface modifications, also

AuNPs can enter tumor cells by a passive mechanism, called enhanced permeability and retention (EPR) effect [46].

Finally, surface charge is also crucial for cellular uptake of NPs, and their stabilization against aggregation. Surface charge affects corona compositions by nonspecific adsorption of serum proteins on NP surface, which alters surface interactions with extracellular proteins when used in cell cultures. For example, citrate-reduced AuNPs have negative charge on their surface due to citrate molecules, or DNA-functionalized AuNPs also have negative surface charge, and when these molecules are used in serum-containing media, serum proteins will adsorb on their surfaces [16, 22]. These negatively charged AuNPs when interact with serum proteins, their uptake half-life, rate and amount will also be affected [22]. In a general view, the cellular uptake is higher for cationic NPs than negative charged NPs, however when oligonucleotides are considered for functionalization of NP surface, the cellular uptake conditions are altered. Despite the need for cationic lipids and polymers for achieving cellular internalization of oligonucleotide-coated AuNPs, Giljohann et al. demonstrated that cellular internalization of Oligo-AuNPs was increased when loading density was also increased, which led to a large number of serum proteins adsorbed on the NP surface [47].

Shape and surface chemistry of AuNPs also affect other biological responses by enhancing the cellular uptake such as induction of apoptosis, damaging DNA, inhibiting angiogenesis, and arresting cell division [48]. Kang et al. demonstrated that Au nanorods conjugated with cell penetrating peptides entered cell nucleus and induced apoptosis by damaging DNA and arresting cytokinesis and cell division [49]. In another study, the surface of AuNPs modified with antibodies that are recognized by vascular endothelial growth factor receptor (VEGFR), which is an essential receptor on the cell surface for angiogenesis, induced tumor cell apoptosis, and inhibited angiogenesis resulted by enhanced cellular uptake [50].

1.2. OLIGONUCLEOTIDE-FUNCTIONALIZED GOLD NANOPARTICLES

AuNPs can be used as a promising delivery vehicle for nucleic acids because of their easy synthesis, monodispersity in colloidal suspension, tunable size, biocompatibility, and ease of surface modification. There are two types of AuNP conjugates as in their design

strategies for nucleic acid delivery: covalent and non-covalent AuNP conjugates [6, 51]. The surface modification of AuNPs used in this study was achieved by covalent binding.

Covalent attachment is achieved by using thiolated oligonucleotides using alkyl thiol adsorption on AuNP surface, which provides a strong S-Au interaction. By using the S-Au binding, the loading capacity of AuNPs, therefore the delivery efficiency is increased [47]. The biological activity is not inhibited from the surface modifications [51-53].

Delivery of nucleic acids such as DNA, ribonucleic acid (RNA), small interfering RNA (siRNA), and short hairpin RNA (shRNA) using nanoparticles (NPs) are used in nanomedicine. One of the most widely studied NPs for nucleic delivery is spherical nucleic acids (SNAs), which are composed of highly oriented and densely packed nucleic acids on metal NP core such as Au (Figure 1.2).

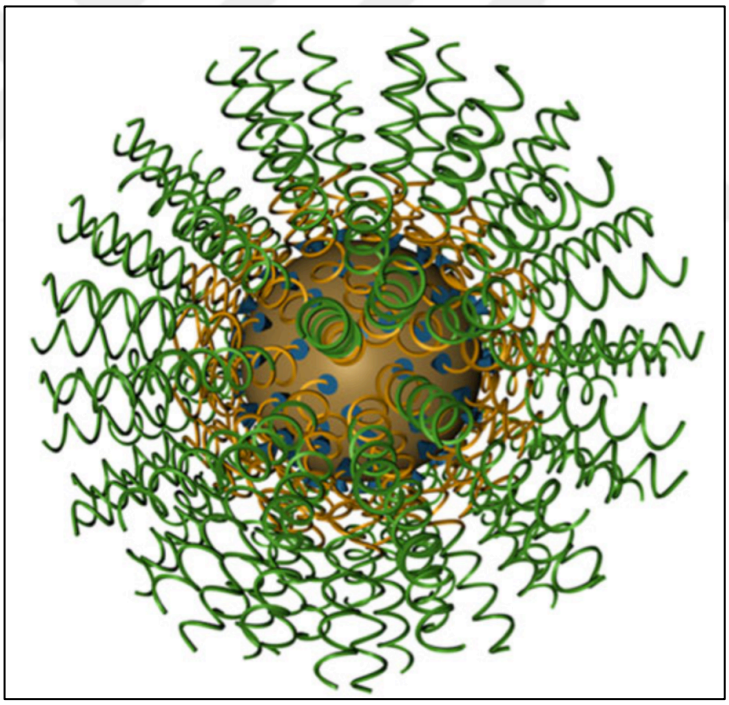

Figure 1.2. SNA nanostructure. Au core is densely functionalized with oligonucleotides, containing an attachment group, a spacer segment and a desired recognition sequence [54].

1.2.1. Biological Responses to Oligonucleotide-Functionalized Gold Nanoparticles

Oligonucleotide-modified AuNPs (Oligo-AuNPs) are widely investigated in many applications such as diagnostic [55] and therapeutic assays [52, 56], intracellular detection [57] and gene regulation [53, 58] due to their enhanced binding and target recognition properties [47, 53]. The effects of Oligo-AuNPs *in vitro* and *in vivo* are being investigated since their introduction in 1996. In 1996, Mirkin et al. proposed a method for surface modification of 13 nm AuNPs using thiolating oligonucleotides [52, 53]. The resulted Oligo-AuNP conjugates had densely packed oligonucleotides on their surfaces, therefore also referred as polyvalent [59]. The length, sequence and composition of the oligonucleotides can be controlled [60].

One of the significant advantages of using AuNPs for oligonucleotide delivery is to prevent or reduce nucleic acid degradation by serum nucleases, and therefore facilitate the passage of Oligo-AuNPs through cell membrane into cells [53, 61]. The increased cellular uptake also provides higher and more efficient delivery of oligonucleotides than conventional transfection agents [53]. The cellular entry of Oligo-AuNPs also affected by the increased serum adsorption on the surface of the AuNPs, which is provided by oligonucleotide functionalization. Giljohann et al. investigated the cellular internalization of Oligo-AuNPs and demonstrated that higher densities of oligonucleotides loaded on the surface of AuNPs also lead to elevated cellular uptake in HeLa, A549 and C166 cells. Moreover, NP-associated serum proteins also enhanced this cellular uptake due to increased number of oligonucleotides attached on the surface of AuNPs [47, 62]. Nucleic acid functionalization had the greatest cellular uptake of AuNPs in HeLa cells, compared to other weakly bound surface ligands, and therefore it proved that stability was crucial for affecting cellular responses, and small changes could have greater impact on cellular level [62]. Patel et al. demonstrated that the uptake mechanism of Oligo-AuNPs was conserved across species and it was mediated by scavenger receptors. Scavenger receptor-A (SR-A) is also a natural binding ligand for poly-G sequences [63].

The increased serum adsorption on Oligo-AuNPs enhanced the cellular uptake, however, also resulted in greater macrophage uptake [47]. The reason for that is mainly because protein corona that is formed due to increased serum adsorption on the surface of NPs. Moreover, the binding of one of the serum protein, opsonin, can be recognized by

macrophages, and lead to increased blood clearance and lower accumulation in target tissues [64-66]. Chinen et al. also demonstrated that G-rich sequences on SNAs enhanced serum adsorption and increased cellular uptake, however also increased the macrophage recognition and uptake when compared to other oligonucleotide sequences. This findings suggested that tertiary structure of oligonucleotides, that were resulted due to G-quadruplex formation, affected the chemical composition of SNA protein corona, and therefore altered cellular response [64].

1.3. NUCLEIC ACID RESEARCH IN NANOMEDICINE

Watson and Crick proposed a simple set of base pairing for four nucleic acid bases: adenine, thymine, guanine and cytosine [67]. Single-stranded DNA has a random coil configuration in normal conditions but when it comes to some specific sequences; well-ordered configurations form [68]. One of the important configurations is that guanine-rich (G-rich) sequences can form G-quadruplex structure when exposed to stabilizing cations (K^+ or Na^+) [69]. In addition to G-quadruplex, as a complementary sequence of guanine: cytosine-rich sequences also exhibit a well-ordered motif depending on the pH of the environment. At an acidic pH, cytosine-rich single-stranded DNA forms i-motif, which is also thermodynamically favored [70]. These self-assembled and stimuli-responsive configurations of specific nucleic acids make them interesting for their use in biomedical applications and nanomedicine [68]. Nanomaterials are intriguing delivery agents for them because sizes of the nucleic acid double helices are approximately 2 nm [68], 0.34 nm is the distance between nucleotides [71], and a typical G-quadruplex structure is approximately 8 nm [72].

For the delivery of nucleic acid using NPs, most preferred ones are carbon-based (carbon nanotubes), metallic (AuNPs, etc.), and cadmium selenide (CdSe) based semi-conductive (Quantum dots, QDs) NPs. Among all NPs suitable for nucleic acid research, AuNPs gain interest due to being inert, biocompatible, and plasmonic. Moreover, using AuNPs as a delivery agent prevents nucleic acid degradation by nucleases and increases stability of oligonucleotides in the presence of serum proteases [53, 55, 57, 58, 68].

Oligonucleotides have the potential to recognize specific sequences and are internalized via clathrin-mediated endocytosis, caveolin-mediated endocytosis and macropinocytosis

[73-75], depending on their charge, shape and sequence-specific interactions [76]. Oligonucleotides have high protein and ligand binding affinity [77-80], they bind to cell surface receptors [81], and modulate cytokine and growth factor activity [82, 83], inhibit cell cycle progression [84].

1.3.1. Guanine-rich Oligonucleotides

Guanines have self-assembly and self-recognition properties, and G-rich oligonucleotides (GROs) have ability to form G-quadruplex structures via Hoogsteen hydrogen bonding in the presence of a cation (Figure 1.3) [85]. G-quadruplexes (also known as G4-DNA) and poly-G regions are found in the human genome [86, 87], and are abundantly distributed in the genome of *C.elegans* [88], and *C. briggsae* [89]. G-quadruplex forming sequences are existed in important regions, such as telomeres [90], regulatory regions of genes such as immunoglobulin switch regions [91], oncogenic promoters [92, 93], and associated with many human diseases such as human immunodeficiency virus (HIV), cancer, and diabetes [94]. They are also highly stable in the presence of cations [95, 96], and resistant to nuclease activity [88, 89], which provide their use for therapeutic medicine.

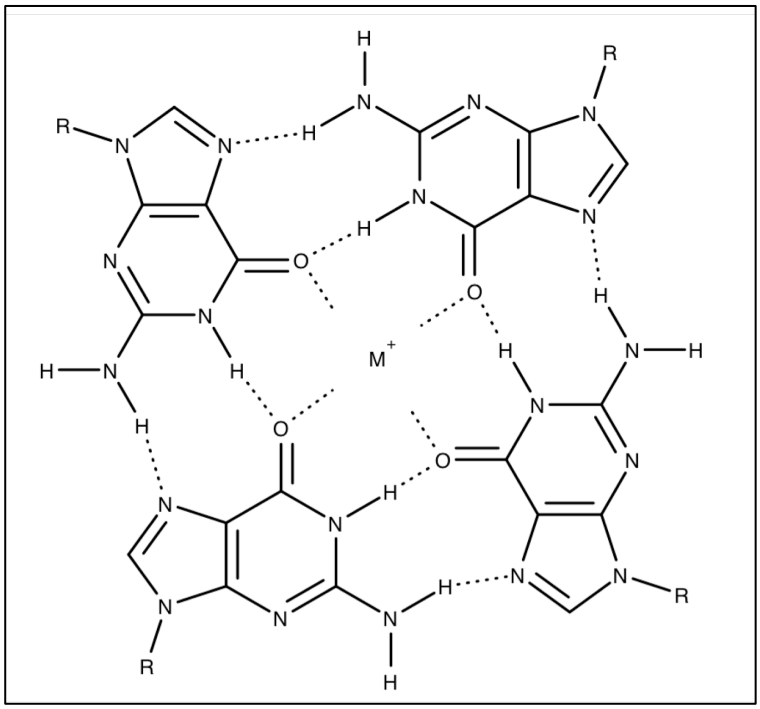

Figure 1.3. The chemical structure of G-quartet. The molecule was drawn by MarvinSketch, Version 15.11.30 (©2015 ChemAxon Ltd.).

One of the important roles of GROs for their use in therapy comes from their ability to prevent telomerase activity, which in turn alter cell cycle progression and selectively induce apoptosis in tumor cells and demonstrate an anti-proliferative effect [78]. GROs were reported previously to show anti-proliferative effects on tumor cells by inhibiting tumor cell growth and recognizing surface receptors for targeting [97-100], as well as nuclease resistance [100], enhanced cellular uptake [100], and alteration of cell cycle progression [101]. Schwartz et al. demonstrated selective killing of malignant esophageal tumor cells and alteration of cell cycle progression using GROs, which consists of monomeric sequence of guanosine [78]. It was found that cells formed sub-G1 population and induced apoptosis when treated with monomeric guanine sequence, while not affected by monomeric A20, T20 or C20.

Above mentioned anti-proliferative effects of GROs are related to their ability to bind to specific surface receptor, and anti-nucleolin antbodies recognize this GRO binding protein. GRO binding protein is defined as nucleolin, or other proteins on the surface of cells which may have same size or similar structure with nucleolin [76]. Nucleolin (110 kDa) is an abundant multifunctional phospho-protein, overexpressed in cancer cells because its level is related to cellular proliferation rate, which is elevated in rapidly proliferating cells such as malignant tumor cells. Hence, nucleolin is a tumor-selective target and it is located predominantly in the nucleus of proliferating cells, as well as GBM, both on the cell surface and in the cell [102, 103]. One of the anti-proliferative G-rich phosphodiester oligonucleotide, AS1411, functions as aptamer (26-mer, 7.8 kDa) to nucleolin, which is developed by Antisoma PLC (London, UK) as an anti-cancer agent and is currently being tested in clinical trials (Phase II) [80]. Bates et al. investigated internalization mechanism of AS1411, and found that AS1411 stimulated macropinocytosis in cancer cells, which is a form of endocytosis, and was found to be mainly dependent on nucleolin [104]. In many studied macropinocytosis was reported as an abundant internalization mechanism of oligonucleotides such as naked DNA, and RNA, also aptamer conjugates [105]. Moreover, normal cells were not stimulated by this type of endocytosis when treated with AS1411, suggesting a cancer-selective uptake of this aptamer [104]. After internalization, AS1411 was accumulated in cancer cells, especially malignant ones, while gradually cleared from normal cells by efflux or exocytosis. In addition, some of the internalized aptamers were

subjected to lysosomal degradation, where selective-accumulation was achieved in cancer cells due to increased retention and enhanced cellular uptake of AS1411 [74].

G-quadruplex forming sequences, and GROs also involve monomeric guanine sequences, and demonstrated to be taken up by cells in increased numbers comparing to other non-guanine sequences, and internalized monomeric guanine sequences (20-mer linear polyguanine, G20) were shown to alter cellular responses such as cell cycle progression, and induction of apoptosis in cancer cells [78]. Narayan et al. studied sequence-specific cellular uptake of SNAs, and showed enhanced cellular uptake of SNAs when modified with linear polyguanine sequences [106]. Moreover, G-quadruplex forming G15-mer oligonucleotides were demonstrated as promising therapeutic carriers when used to form thin multilayer films and microcapsules [107]. Sengar et al. further investigated the structure of various long polyguanine sequences, and suggested a well-resolved structural characterization of G15-mer sequences using nuclear magnetic resonance (NMR) due to well-defined G-quadruplex structure formed by poly-G sequences [108]. In addition to these structural chemical studies, Lubitz et al. studied G4-DNA (G5, G10, and G20) functionalized AuNPs, and demonstrated highly stable NPs, and these NPs assembled into unique structures, NP-flower due to increased G-tetrad numbers and interparticle separation distance [109, 110].

1.4. BRAIN TUMORS AND GLIOBLASTOMA

Brain tumors are approximately 1.4 per cent of all cancers, and cause for 2.3 per cent of all cancer-related death [111]. According to World Health Organization (WHO), brain tumors are classified depending on their invasiveness and malignancy from I to IV, where grade I refers to benign tumors and IV malignant ones. Types of brain tumors are gliomas (astrocytomas, oligodendrogliomas, ependymomas), meningiomas, medulloblastomas, gangliogliomas, schwannomas, and chordomas [112]. Majority of brain tumors are astrocytomas, which are also called glioblastoma (GBM), grade IV, according to WHO [113].

Novel therapeutic targets for drug and small molecule delivery, gene and viral therapy, as well as immunotherapy gain interest for brain tumor research last two decades. Especially, BBB-targeted delivery and combined therapies are being studied for delivery of the

cytostatic drugs such as doxorubicin (DOX), temozolomide (TMZ), paclitaxel, cisplatin, carboplatin, etc. to tumor locations using novel technologies. In high-grade tumors BBB becomes leaky so drugs can pass, but in low-grade tumors drug delivery is crucial due to intact BBB. Hence, enhanced targeting and efficient delivery of drugs are needed and achieved by lipidizing drugs, using liposomes as nanocarriers, etc. for the delivery of cytostatic drugs such as DOX, TMZ, and paclitaxel [114, 115].

1.4.1. Glioblastoma

Among all primary brain tumors, gliomas are the most abundant ones and 70-75 per cent of these tumors developed from astrocytes, which are the most numerous and diverse glial cells in the central nervous systems (CNS) [111, 116]. Glioblastoma (GBM) is a highly aggressive brain tumor, which is mostly seen in adults, and have poor prognosis with a rapidly growing neoplasms that can cause death in a year [117-119]. The characteristics of GBM includes dense cellularity, high proliferation and necrosis [111].

Telomerase activity is also important characteristics of malignant cancer types, and therefore telomerase activity is therefore crucial for differentiation of cancer cells [120], as well as for tumor immortalization [121]. Telomerase is a ribonucleoprotein and a restrictive enzyme, which prevents telomeres from being shortened. Telomeric chromosome regions contain G-rich repeats ($TTAGGG_n$), which is added by telomerase and stabilizes the chromosome [122]. In cancer therapy, G-quadruplex forming sequences, therefore, become important for preventing both telomerase activity and alternative lengthening of telomere (ALT), which is a much less common mechanism for telomere shortening [123].

Telomerase activity has been identified in cancer cells, mostly in malignant cancer types including GBM [124-126], where normal adjacent tissues are negative for telomerase activity [127, 128]. However, telomerase activity depends on the tumor type; for example some pediatric GBM lack telomerase activity and maintain telomeres via ALT [129]. In 2003, Hakin-Smith et al. found that ALT phenotype is a good prognostic marker in GBM [130].

Current therapies of GBM involve neurosurgical resection of tumor lesions, radiotherapy and chemotherapy with the drug TMZ, and other combinations of cytostatic drugs [131]. The poor prognosis of GBM is mainly related to disrupted BBB, which becomes leaky and lesions are resistant to many conventional therapeutic drugs and complete removal of the tumor is very difficult without damaging any surrounding normal tissues. The integrity of brain is altered with the disrupted intercellular junctions, enzyme systems and selective transport of BBB (Figure 1.4). The leaky and disturbed BBB in GBM is a major obstacle for its therapy even if drugs can pass through the barrier in high-grade tumors, tumor cells gain resistance to chemotherapy [111, 132].

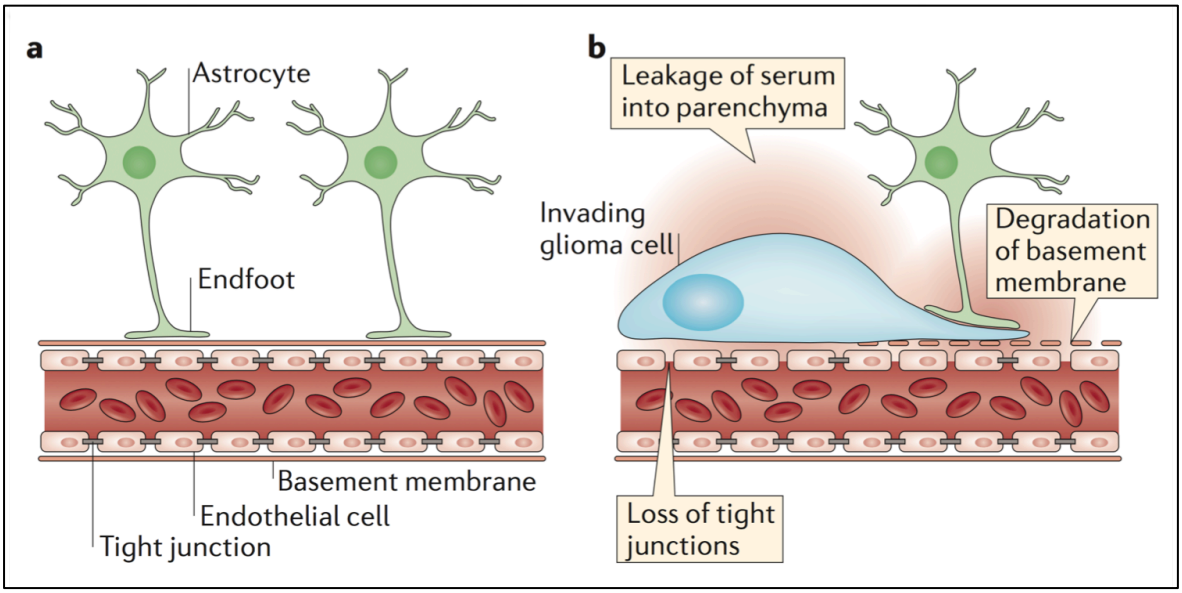

Figure 1.4. Disruption of BBB caused by glioma cells. (a) Intact BBB in healthy brain; blood vessels are surrounded by astrocytic end-feet, and BBB is formed by vascular endothelial cells through tight junctions, (b) Disrupted and leaky BBB in GBM; astrocytic end-feet is displaced by invading glioma cell, results in loss of tight junctions and BBB structure is altered [133].

Nanomedicine aims to overcome this issue by using NPs for enhanced targeting of tumors, selective targeting of receptors, selective killing of the tumors, and tagging the NPs with fluorescent marker for the simplified imaging of tumors [111, 134, 135]. For achieving the facilitated delivery across BBB, and enhanced targeting delivery with minimum elimination of NPs from bloodstream via reticuloendothelial system (RES), NPs should have important characteristics such as size, hydrophobicity, and surface charge [136].

1.5. GOLD NANOPARTICLES AND GLIOBLASTOMA

1.5.1. Gold Nanoparticles and Brain

The brain is isolated from general blood circulation via blood-brain barrier (BBB), which is composed of astrocytes, neurons, pericytes, and vascular endothelial cells connected by tight junctions [137]. The BBB maintains homeostasis of central nervous system (CNS) and regulates the passage of circulating macromolecules from brain-to-blood or vice versa depending on their physical properties such as size, charge and hydrophobicity [111].

Lipid-soluble, hydrophobic molecules can diffuse across BBB using endothelial cells, while water-soluble, hydrophilic molecules transport across BBB through tight junctions. Additionally, small molecules can penetrate the BBB through carrier- mediated transport easily, while large molecule transportation needs receptor-mediated transcytosis. Moreover, when surface charge is considered, cationic molecules can enter easily by adsorptive-mediated transcytosis or endocytosis, while the entry of negative molecules are mainly inhibited [111, 137].

The BBB is permeable to AuNPs having size up to 200 nm, according to several studies [138-142]. Particle size, as well as the surface chemistry of these nanoparticles affects their biodistribution and accumulation in different tissues [48, 142, 143]. When size of AuNPs increased (100 to 200 nm), only trace amounts of AuNPs were detected in brain, and the maximum accumulation in brain was achieved by 15 nm AuNPs [138, 144]. The reason for that can be related to the distance between astrocytic end-feet of brain astrocytes and the capillary endothelium, which is only 20 nm [145]. In the case of 50 nm, accumulation of AuNPs in brain was also detected, but with a decreased amount [138].

1.5.2. Gold Nanoparticles for Glioblastoma Therapy

AuNPs are the most widely adopted nanomaterials for GBM therapy, and one of the most preferred technique for GBM therapy is to introduce AuNPs with either X-rays or gamma-rays to increase the effectiveness of radiation therapy [146]. By using this targeted radiation, Joh et al. showed enhanced accumulation of AuNPs in GBM tumors via the

disrupted BBB (Figure 1.5) [139]. Hainfeld et al. also used this approach *in vivo* for glioma treatment, compared with radiation-only group, and demostrated that X-rays combined with non targeted AuNPs was a better therapy than that of only radiation [140].

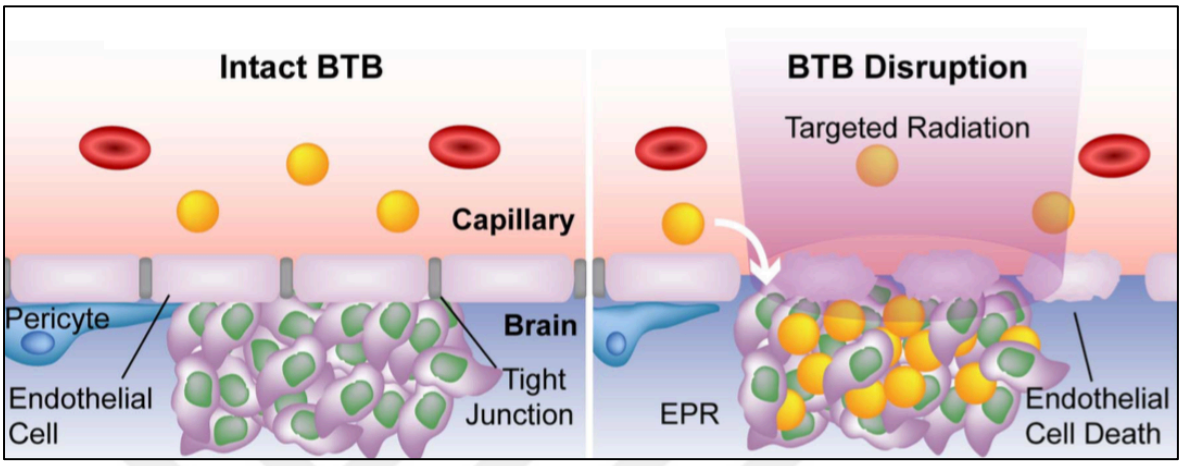

Figure 1.5. Schematic of radiation-induced disruption of BBB [139].

Combinational therapies other than the use of electromagnetic radiation include PTT and drug delivery. PTT utilize visible, infrared, or radiofrequency pulses in order to heat AuNPs to cause damage on tumor cells [147-149]. There are several studies in which brain tumors are studied for PTT, and radiation therapy using AuNPs. Kang et al. studied PTT for brain cancer therapy using pH-sensitive AuNPs, and demostrated enhanced targeting and anti-cancer effect upon heat generation in glioma-bering mice *in vivo* [150]. In a previous study, Madsen et al. used macrophage-loaded gold nanoshells for PTT of glioma, and also showed anti-proliferative effects, and enhanced targeting within glioma spheroids *in vitro* [151]. Bobyk et al. showed distinctive DNA damage in F98 glioma cells *in vitro* when AuNPs were applied prior to radiation, and resulted in increased survival of glioma-bearing rats after the combinational treatment of AuNPs and electromagnetic radiation *in vivo* [152].

An AuNP-based drug delivery for glioma therapy was demonstrated in a recent study [153]. Ruan et al. showed an effective accumulation of polymer-coated and DOX-loaded AuNPs in glioma cells *in vitro*. Additionally, the group also demostrated that glioma-bearing mice, which were treated with the same nanoparticles had longer survival time than control group. Another research group used silica-coated AuNPs for the delivery of TMZ and DOX into U87MG cells, and showed an effective delivery to GBM cells than

direct delivery of the drugs [154]. Meyers et al. combined peptide-targeted AuNPs and photodynamic drug, Pc 4, in order to improve drug delivery, and increase efficiacy of targeted delivery over untargeted drug delivery. The study suggested peptide-modified AuNPs could successfully target brain tumor in a mouse model of GBM, hindered tumor growth, hence, resulted in a decrease in tumor size [155].

Surface chemistry of AuNPs is crucial for their use in nanomedicine, and for GBM therapy, AuNPs can be modified with various types of biomolecules such as cell penetrating peptides, proteins, antibodies, enzymes, carbohydrates, and oligonucleotides [156-158]. Ruan et al., used peptide-modified AuNPs to improve their accumulation in GBM, and showed that RGD-modified AuNPs transcytosized across BBB via integrin $\alpha_v\beta_3$ receptor which was located on BBB, and efficiently accumulated in GBM site. After NPs entered into cells, they formed aggregates in the extracellular matrix and in the endosome/lysosome via overexpressed legumain (a protease expressed in tumor cells), which in turn limited their exocytosis by cells [159]. The same group previously demostrated legumain-triggered aggregation of AuNPs in glioma cells both *in vitro* and *in vivo*, and this aggregation resulted in enhanced retention of chemotherapeutics and provided higher accumulation of NPs in glioma site [160].

For an effective treatment of GBM, BBB and blood tumor barrier (BTB) permeability is a major issue, and AuNPs are crucial for GBM research due to their penetration across these biological barriers (Figure 1.6) [137]. Moreover, one of the most BBB permeable and widely studied approach in nanomedicine for cancer therapy is the delivery of nucleic acids using AuNPs [161]. SNAs are more efficient than the traditional nucleic acid delivery, resistant to degradation by serum nucleases, and no other transfection agents are necessary for their delivery. SNAs, also known as polyvalent oligonucleotide-modified AuNPs, are used to deliver double stranded DNA (dsDNA), single-stranded DNA (ssDNA), microRNA (miRNA) and siRNA [162-164]. Jensen et al. used *Bcl2L12*-specific SNAs (siL12-SNAs) as an RNAi-based therapy for GBM. Bcl2L12 is targeted because it is overexpressed in GBM, and results demostrated an effective gene silencing (knock down of B*cl2L12* mRNA), reduced protein levels, and induced apoptosis via p53 and effector caspase activity [158]. In addition, Kouri et al. synthesized miR-182 functionalized AuNPs (182-SNAs), which penetrated through BBB and BTB in GBM xenograft models and reduced tumor burden, resulting the number of survived animals. These studies of using

SNA-based transfers suggests a promising strategy for targeting multiple oncogenes such as *Bcl2L12*, *c-Met*, and hypoxia-inducible factor 2α (*HIF2A)* [165].

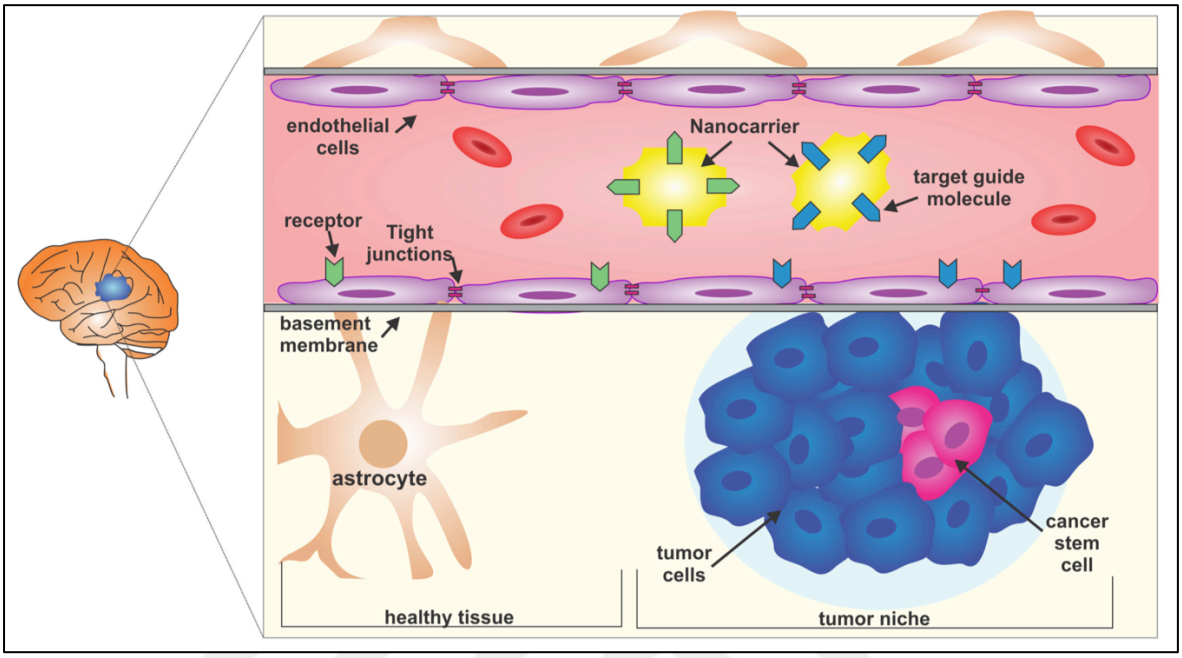

Figure 1.6. GBM tumor niche, and a possible strategy to reach glioma cells using targeted nanocarriers through the BBB [132]. AuNPs are used for targeting brain markers [132], gene therapy [158], imaging [140], and PTT [152, 166].

Using G-rich aptamers as therapeutic agents, has some advantages over other oligonucleotide-based approaches due to their enhanced cellular uptake and highly heat-stable stucture [64, 123]. G-rich aptamers are also non-immunogenic, and show increased resistance to serum nucleases [74]. One of the important G-rich phosphodiester oligonucleotide is AS1411, which is developed by Antisoma PLC (London, UK) and is being tested as an anti-cancer agent in Phase II clinical trials. AS1411 functions as aptamer to nucleolin, and U87MG [167], and SF-268 cells [168] (GBM cell lines) are shown to be responsive to AS1411. In a recent study, Dam et al. functionalized the surface of gold nanostars with nucleolin-specific AS1411 DNA aptamer, and demostrated apoptosis induction and increased cell death via caspase 3/7 activity in cancer cells, incuding GBM [169]. Mirkin and colleagues, reported AS1411-coated AuNPs enhanced cellular uptake and increased serum adsorption, when compared to both unconjugated oligonucleotides and other non-G-rich oligonucleotides [64]. However, G-rich oligonucleotide modified

AuNPs or AuNPs modified with G-quadruplex forming sequences have not been studied for GBM therapy yet.

1.6. AIM OF THE STUDY

Surface functionalization of AuNPs using GROs and G-quadruplex forming sequences are being studied, however, little is known about the biological responses of these potential therapeutic carriers. In this study, cellular responses such as cell viability, cell cycle alteration, apoptosis induction, and cellular uptake of polyguanine-modified oligonucleotides were investigated in NHA, U373 and U87MG cells. Moreover, in order to demonstrate how slight changes in surface chemistry of AuNPs can significantly impact its cellular response, AuNPs were modified with two different monomeric guanine sequences, which differ only in length. Length-dependent cellular responses using polyguanine-modified AuNPs revealed S-phase arrest, enhanced cellular uptake, and increased apoptosis induction in GBM cells while normal cells were not affected, demonstrating selective killing of GBM cells. This study highlights small changes on the surface of nanoparticles such as guanine base length can significantly affect its biological response in GBM cells, and these findings are crucial for the use of monomeric polyguanine-modified AuNPs as therapeutic carriers in GBM therapy.

2. MATERIALS

2.1. CHEMICALS AND REAGENTS

Gold (III) chloride trihydrate ($HAuCl_4 \cdot 3H_2O$, MW: 393.83 g/mol; Sigma-Aldrich #520918 USA), trisodium citrate dihydrate ($C_6H_5Na_3O_7 \cdot 2H_2O$, MW: 294.10 g/mol; Merck #A829748 Germany), ortho-phosphoric acid (H_3PO_4, 85 per cent, d: 1.71 g/cm^3, stock: 14.8 M; Merck #100573 Germany), potassium phosphate dibasic (K_2HPO_4, MW: 174.18 g/mol; Sigma-Aldrich P3786 USA), sodium dodecyl sulfate (SDS, $C_{12}H_{25}O_4SNa$, MW: 288.38g/mol; Bio Basic Inc. #151213 Canada), sodium chloride (NaCl, MW: 58.44 g/mol; Sigma-Aldrich #31434 USA) were used for chemical synthesis, characterization and functionalization of gold nanoparticle surface. All glassware were cleaned using aqua regia (HCl:HNO_3 of 3:1). For the preparation of aqua regia, nitric acid (HNO_3, 65 per cent; #84378) and hydrochloric acid (HCl, 37 per cent; #30721) were purchased from Sigma-Aldrich, USA.

Dulbecco's modified Eagle medium (1X DMEM, 4.5g/L D-Glucose, L-glutamine, sodium pyruvate; Gibco #11965092 USA), Dulbecco's modified Eagle's medium Nutrient mixture F-12 Ham (DMEM/F-12, 1:1 mixture; Sigma-Aldrich #D6421 USA), Dulbecco's modified Eagle medium (1X DMEM, 4.5g/L, D-Glucose, L-glutamine, 25 mM HEPES, no phenol red; Gibco #21063029 USA), fetal bovine serum (FBS, Gibco #10270 UK), HyClone™ phosphate buffered saline (10 X PBS, w/o calcium, magnesium Gibco #SH30256 USA), Pen-Strep (10,000 Units/ml penicillin, 10,000 μg/ml streptomycin; Gibco #15140122 USA), L-glutamine (200 mM; Gibco #25030024 UK), 0.25 per cent trypsin-EDTA (1X, Gibco #25200056 UK), sodium pyruvate (100 mM, Gibco #11360070 USA), dimethyl sulfoxide (DMSO, ≥99.9 per cent; Sigma-Aldrich #472301 USA), colchicine (≥95 per cent (HPLC); MW: 399.44 g/mol; Sigma-Aldrich #C9754 USA), propidium iodide solution (PI, 1.0 mg/ml in water; Sigma-Aldrich #P4864 USA) Ribonuclease A (from Bovine pancreas, ≥70 Kunitz units/mg protein; Sigma-Aldrich #R6513 USA), ethanol (≥99.8 per cent (GC); Sigma-Aldrich #32221, USA) and 2-propanol (99.5 per cent; Sigma-Aldrich #24137 USA) were used for further cell culture maintenance and cellular assays.

For *in vitro* cellular toxicity experiments, Annexin V-FITC Early Apoptosis Detection Kit (Cell Signaling Technologies #6592 USA) and Cell Proliferation Reagent WST-1 (Roche #05015944001 USA) were used in this study. Annexin V-FITC Early Apoptosis Detection Kit #6592 included PI staining solution #20X11733S, Annexin V-FITC Conjugate #4984S and 10X Annexin V Binding Buffer #11732S.

Ultrapure water (18.2 MΩ.cm at 25^{o}C) used for glassware cleaning and gold nanoparticle synthesis was purified using a Millipore Direct-Q® water purification system throughout this study.

2.2. OLIGONUCLEOTIDES

All oligonucleotide sequences used in this study for surface modification, were synthesized by Alpha DNA (Montreal, QC, Canada). Sequences used for AuNPs surface modification were listed in Table 2.1.

Table 2.1. Oligonucleotide sequences used for surface modification.

Sequence No	Name	Sequence (5' to 3')	Length	Modification
1	G10-AuNPs	GGG GGG GGG GAA AAA AAA AA	20	3'-end thiol
2	G20-AuNPs	GGG GGG GGG GGG GGG GGA AAA AAA AAA	30	3'-end thiol

Lyophilized oligonucleotides were used to prepare 100 μM stock solutions.

2.3. INSTRUMENTATION

Autoflow IR direct heat CO_2 incubator (37^{o}C, CO_2 five per cent, Nuaire, USA), Biohazard safety cabinet (Esco Class II type A2, USA), waterbath (Isolab Laborgeräte GmbH, Germany), light microscope (Nikon Eclipse TS100, UK), Sigma 2-5 centrifuge (UK), mikro 22 R centrifuge (Hettich, UK), programmable mini-shaker (BioSan, Latvia), vortex (Heidolph Instruments, Germany), ultrasonic bath (Bandelin Sonorex, Germany), pH meter

(HI2211, Hanna Instruments, UK), mini centrifuge (Galaxy MiniStar, VWR, Korea), heater (Isolab Laborgeräte GmbH, Germany), PowerPac™ Basic power supply (Bio-Rad, USA), horizontal gel electrophoresis tank (Cleaver Scientific, UK), UV/Vis Spectrometer (Lambda 25, Pelkin Elmer, USA), Zetasizer Nano ZS (Malvern Instruments, UK), Atomic Force Microscopy (AFM, Park Systems XE-100, Korea), Transmission Electron Microscopy (TEM, JEM-2100, Jeol USA, Inc., USA), Nicolet™ iS50 FT-IR (ThermoFisher Scientific, USA), ELx800 Absorbance Reader (Biotek, USA) and Guava easyCyte™ flow cytometer (Millipore, USA) were used in this study.

2.4. CELL LINES

NHA (normal human astrocytes) was provided by Assist. Prof. Dr. Hüseyin Çimen, Proteomics and Mass Spectrometry (YediPROT) Laboratory, Yeditepe University Faculty of Engineering and Architecture, Department of Genetics and Bioengineering, Istanbul, Turkey. U87MG and U373 GBM cell lines were kindly provided by Assist. Prof. Dr. Tuğba Bağcı Önder, Brain Cancer Research and Therapy Laboratory, Koç University School of Medicine, Istanbul, Turkey.

3. METHODS

3.1. SYNTHESIS OF GOLD NANOPARTICLES

Synthesis of 13 nm gold nanoparticles (AuNPs) was performed according to Turkevich method [2]. 160 µl from 500 mg/ml stock solution of gold (III) chloride trihydrate (400µg/ml; 1 mM) was added into 200 ml ultrapure water and the solution was heated. Meanwhile, 38.8 mM trisodium citrate solution was freshly prepared. When, boiling point was reached, 20 ml (10 per cent v/v) of 38.8 mM trisodium citrate solution was quickly added into the boiling solution, while it was stirred. The volume of final trisodium citrate added into the solution was approximately 10 per cent of the total volume of the solution for the synthesis of AuNPs with an average size of 13 nm [3]. The color of the solution was first turned into colorless from pale yellow when trisodium citrate solution was added, then colorless turned into black. When the color of the solution turned into ruby red from black, and started boiling again, it was kept under reflux for 15 min. Then, gold nanoparticle suspension was allowed to cool to the room temperature (RT).

UV/Vis spectroscopy was used for estimation of colloidal concentration of synthesized nanoparticles. The concentration of resulting 13 nm colloidal gold was calculated as 14 nM according to Beer's Law. Extinction coefficient of 13 nm AuNPs at 520 nm is $2.7\times 10^{8}\ M^{-1}\ cm^{-1}$ [143, 170-172].

3.2. SURFACE FUNCTIONALIZATION OF GOLD NANOPARTICLES

Lyophilized oligonucleotides were used to prepare 100 µM stock solutions using ultrapure water and stored at -20^{o}C. Lyophilized oligonucleotides were first spun down and then dissolved in ultrapure water. The stock solutions were sterilized at 65^{o}C for 10 min.

Prior to surface functionalization studies, the optimizations for SDS percentage, phosphate buffer (pH 7.4) amount and NaCl concentration were performed. The modification method, which had reproducible spectral bands for Oligo-AuNPs was considered as optimized. SDS was used to prevent the AuNPs from adhering either to each other or to the wall of the

reaction tubes, and NaCl additions were used to increase the loading capacity of oligonucleotides [172].

Gold colloidal suspension (approximately 14 nM) was adjusted to 0.01 M phosphate buffer (pH 7.4) and 0.1 per cent SDS before performing oligonucleotide addition. Approximately 2 nmol thiol-modified G10-AuNPs and G20-AuNPs (20 µl) were added to citrate stabilized 13 nm gold nanoparticles. After the addition of 20 µl from 100 µM stock solutions of oligonucleotides, the colloidal suspensions were sonicated for 30 seconds and gently shaken for 30 min. After 30 min, step-by-step salt addition was performed using 2.0 M NaCl for salt stabilization. First, the resulting salt concentrations in colloidal suspensions were brought to 0.15 M. Then, two more salt additions were performed in 30-min intervals to bring the final salt concentration to 0.25 M while colloidal suspensions were gently shaken throughout these processes and sonicated for 30 seconds after each salt addition. Resulting oligonucleotide modified-AuNPs were gently shaken overnight. To remove unbound oligonucleotides, colloidal suspensions were centrifuged at 13,000 rpm at 25^{o}C for 30 min for three times and each time washing was performed using sterile 1X PBS solution (Figure 3.1). The surface modified-AuNPs did not show any aggregation after five days, confirming its stability after the NaCl additions.

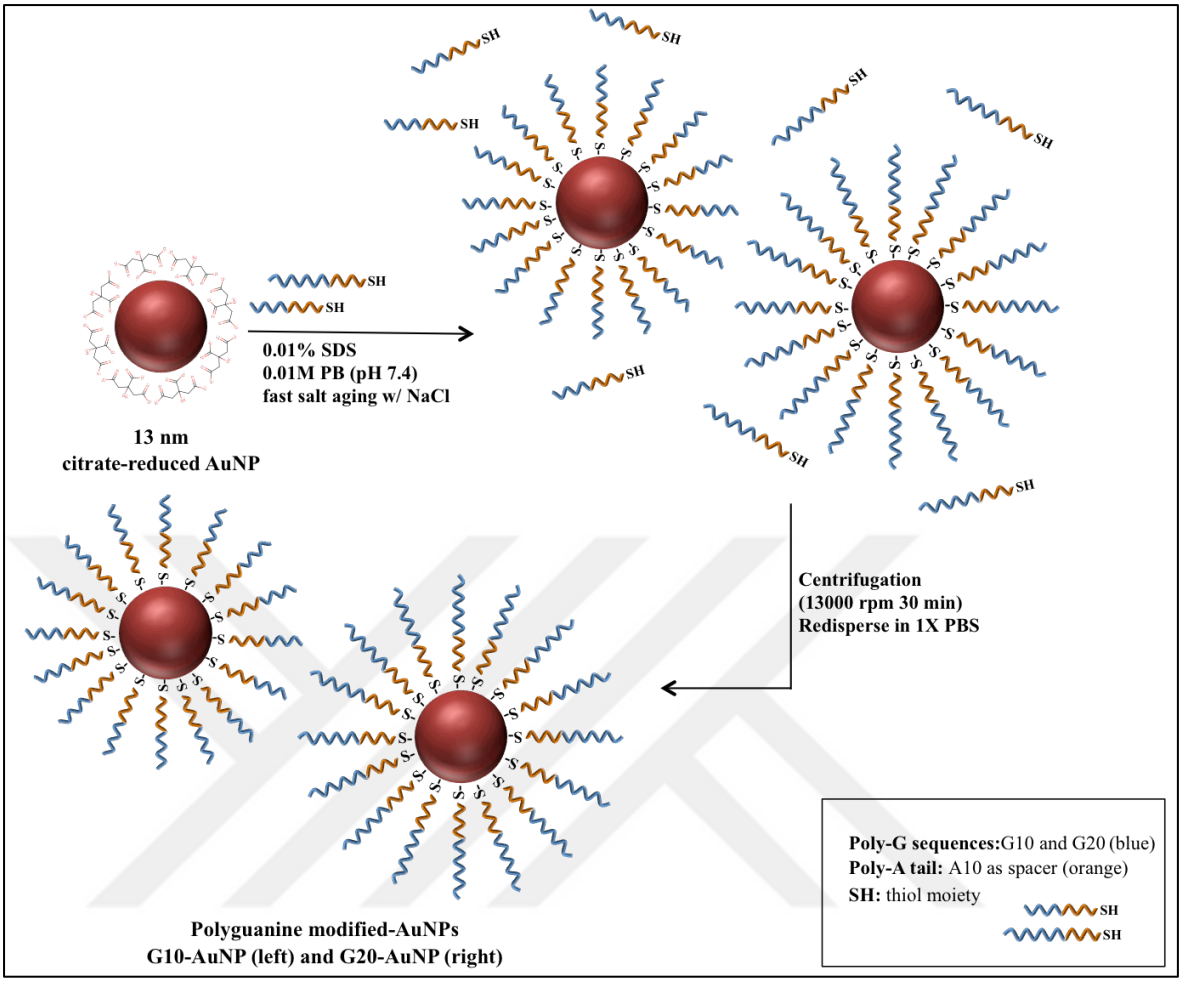

Figure 3.1. Schematic drawing of the fast salt aging method for surface functionalization of 13 nm citrate-stabilized AuNPs using thiolated poly-G sequences. Poly-A-tailed G10 and G20 sequences were added to citrate-stabilized gold colloid, and attached on gold surface via alkyl thiol adsorption. Prior to the addition of oligonucleotides, gold colloid was adjusted to 0.01% SDS and to 0.01M phosphate buffer (pH 7.4) for maximized surface functionalization. For further purification, centrifugation was performed.

3.3. CHARACTERIZATION OF GOLD NANOPARTICLES

3.3.1. UV/Vis Spectroscopy

Synthesized citrate-reduced 13 nm AuNPs and oligonucleotide-functionalized AuNPs were characterized by UV/Vis Spectrometer (Lambda 25). Samples were diluted in water and transferred into 1.5-ml quartz cuvette, which has 1-cm path length. Their SPR absorption spectra were recorded in the range from 300 to 800 nm.

3.3.2. Dynamic Light Scattering and Zeta-Potential Measurements

Zeta (ζ) potential distribution and average hydrodynamic size measurements were conducted using Malvern Zetasizer Nano ZS at 25°C, and the refractive index and absorption of AuNPs were adjusted to 2.0 and 0.32, respectively. Disposable polystyrene cuvettes were used for DLS measurements, and cuvettes were washed with ethanol and pure water prior to ζ-potential measurements.

3.3.3. Transmission Electron Microscopy

The size, morphology and monodispersity of citrate-reduced 13±3 nm AuNPs were examined using High Resolution Transmission Electron Microscopy measurements (TEM) at 200 kV. Samples were placed on a holey carbon TEM grid and were imaged by TEM (JEOL-2100 HRTEM).

3.4. CELL CULTURE MAINTENANCE

U87MG (passage 13 to 19) and U373 (passage 15 to 22) GBM cells were maintained in DMEM containing 10 per cent v/v FBS and one per cent v/v Pen-Strep. On the other hand, for NHA (passage 12 to 18), DMEM/F-12 containing 50 per cent v/v FBS and one per cent v/v Pen-Strep was used. Cells were incubated in CO_2 incubator at 37^{o}C, which is supplied with five per cent CO_2. Cells were cultured in T25 and T75 flasks at different seeding densities.

3.5. *IN VITRO* CELL PROLIFERATION ASSAY

Cells were seeded at density of 1.0 x 10^4 cells/well in a 96-well tissue culture plate. Cells were allowed to attach for 24 h prior to treatment. Media was replaced with freshly prepared NPs and cells were treated with various concentrations of AuNPs, G10-AuNPs, and G20-AuNPs for 24, 48 and 72 h. DMSO (10 per cent) was used as positive control. Cell viability was determined using WST-1 Cell Proliferation Reagent kit, according to manufacturer's protocol. This method of determining cell viability is based on the cleavage of WST-1, which is a tetrazolium salt, and formation of formazan by mitochondrial dehydrogenases. Briefly, after 24, 48, and 72 h of treatments were accomplished, media in each well was replaced by 100 µl of fresh one, including 10 per cent v/v of WST-1 in it. After well were incubated at 37^{o}C in CO_2 incubator (CO_2 five per cent) for approximately 40 minutes, absorbance values at optical density (OD) of 450 nm were measured using microplate reader. Experiments were performed in triplicate.

3.6. DETECTION OF THE CELL CYCLE DISTRIBUTION

To determine the cell cycle distribution, U87MG and U373 GBM cells and NHA were seeded at a density of 2.5 x 10^4 cells/well in a 24-well tissue culture plate and collected after 24 h treatment of 2.5 nM AuNPs, G10-AuNPs, and G20-AuNPs. As a positive control, cells were also treated with 0.1 µM colchicine (a mitotic inhibitor [173]) to arrest the cells in G_2/M phase, and as negative controls, untreated cells were used for gating. Collected cells were washed twice with sterile 1X PBS and fixed in 70 per cent ice-cold ethanol at -20^{o}C overnight. Fixation was performed drop-by-drop addition of 300 µl of cell suspensions in 700 µl 100 per cent ethanol. During the fixation process addition of cell suspensions was performed under gentle vortexing in order to prevent clumping of the cells. Fixed cells were centrifuged twice at 3,000 rpm for 10 min at 4^{o}C. After removal of ethanol, cells were labeled with 0.05 per cent PI (from 1 mg/ml stock) in the presence of 0.1 per cent Rnase A (from 1 mg/ml stock) for 30 min on ice. Cell populations in G_0/G_1, S and G_2/M phases were analyzed by Guava easyCyte™ flow cytometer. Experiments were performed in triplicate.

3.7. CELLULAR UPTAKE STUDIES AND NANOPARTICLE CALCULATIONS

For cellular uptake studies, a spectroscopic method was performed [174]. Cells were seeded at a density of 2.5 x 10^4 cells/well in a 24-well tissue culture plate. Next day, 2.5 nM G10-AuNPs and G20-AuNPs were prepared in phenol red-free media, and prior to any incubation, prepared media were used for UV-Vis measurements. Phenol red-free media (complete; with antibiotics and FBS) was used as a background. Cells were washed with 1X PBS to remove phenol, and treated with these NPs, and after 24 h media, and two extra washes were collected to collect all loosely bound-NPs on the cell surface, and used for a second UV/Vis measurement. Cells were also trypsinized and counted with hemocytometer for further cellular uptake calculations. The experiments were performed in triplicate, and unmodified AuNPs were not used in this uptake study due to its aggregation, and the black-purple color resulted from this aggregation interfered the spectroscopic uptake measurements.

Nanoparticles taken per cell (*N*) were calculated using a basic knowledge about gold colloidal suspensions. According to literature, AuNPs (~13 nm) has an average number of 10^{12} nanoparticles per ml, which was calculated using Avogadro's number ($6x10^{23}$ particles/liter) [22, 175-177]. Moreover, the concentration of gold colloidal suspension was calculated as approximately 14 nM via Beer's Law, using extinction coefficient of 13 nm AuNPs at 520 nm.

3.8. DETECTION OF APOPTOTIC CELLS

To investigate whether AuNPs and Oligo-AuNPs induce apoptosis in U87MG, U373 GBM cells and NHA, Annexin V-FITC early apoptosis detection kit was used, according to manufacturer's protocol. For this assay, cells were seeded at a density of 2.5 x 10^4 cell/well in a 24-well tissue culture plate and treated with 2.5 nM AuNPs and 2.5 nM G10-AuNPs, and G20-AuNPs for 24 h. Cells were also treated with 10 per cent DMSO as a positive control, because most of the drugs (TMZ, etc.) used for GBM treatment is soluble in DMSO, and gating was performed using untreated cells as negative control. After 24 h treatment, cells were harvested and washed twice with sterile 1X PBS in order to remove media, and final washing step was performed with ice-cold PBS. Then, cells were stained

to quantify induction of apoptosis using Annexin V-FITC Early Apoptosis Detection Kit (CST) following manufacturer's recommended protocol. Briefly, after washing collected cells with ice-cold 1X PBS, cells were resuspended in 1X Annexin V Binding Buffer, following a 10-minute staining procedure on ice with 1:12.5 ratio of Annexin V-FITC conjugate and Propidium Iodide (PI). Then, cells were analyzed by Guava easyCyte™ flow cytometer. Experiments were performed in triplicate.

3.9. STATISTICAL ANALYSIS

All experimental data were expressed as the mean ± standard deviation of at least three independent experiments. Significant differences between two groups were analyzed using a 2-tailed, paired t-test in Microsoft® Excel® for Mac 2011 Version 14.4.8, and $p<0.05$ was considered to be statistically significant.

4. RESULTS

4.1. CHARACTERIZATION OF GOLD NANOPARTICLES

The synthesized AuNP colloidal suspension was characterized using DLS and UV/Vis spectroscopy and (Figure 4.1). From UV/Vis spectrum, surface plasmon resonance (SPR) of AuNPs was characterized, and AuNPs exhibited a distinctive maxima at 520 nm, which is a characteristic λ_{max} of 13 nm spherical AuNPs (Figure 4.1A). The DLS spectrum of the colloidal suspension of AuNPs showed an average hydrodynamic size of 13 nm (Figure 4.1B).

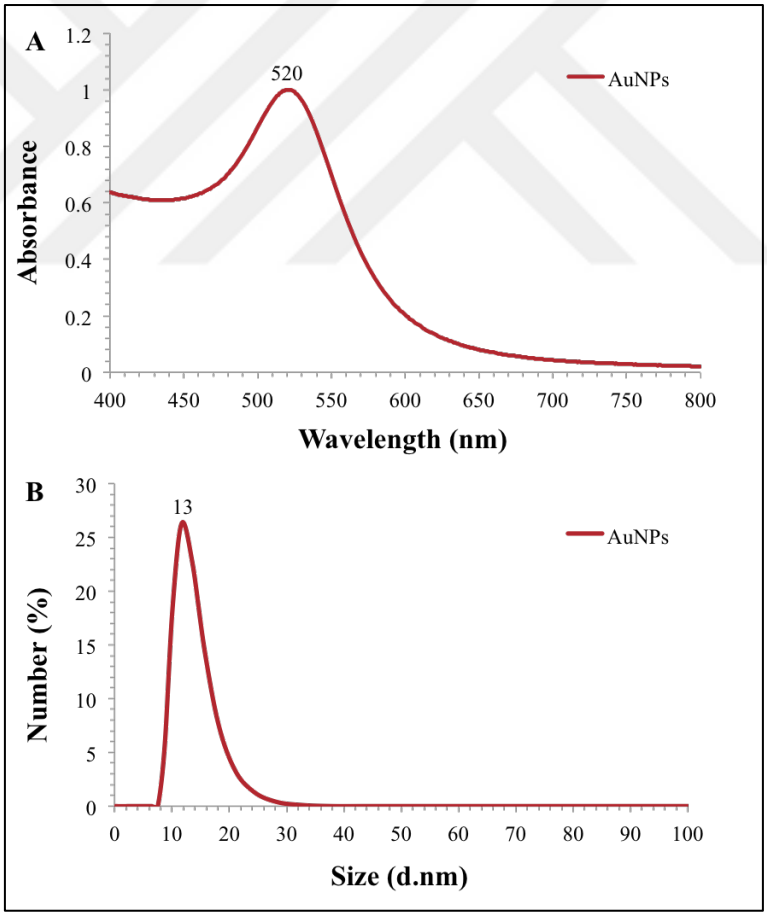

Figure 4.1. Characterization of citrate reduced-AuNPs. (A) UV/Visible spectrum of AuNPs and (B) DLS datum showing average hydrodynamic size of AuNPs.

The size, morphology and monodispersity of citrate-reduced AuNPs were examined using Transmission Electron Microscopy measurements (TEM) and image can be seen in Figure 4.2. Citrate-reduced AuNPs had an average size of 13±3 nm and nanoparticles had high monodispersity with spherical shapes.

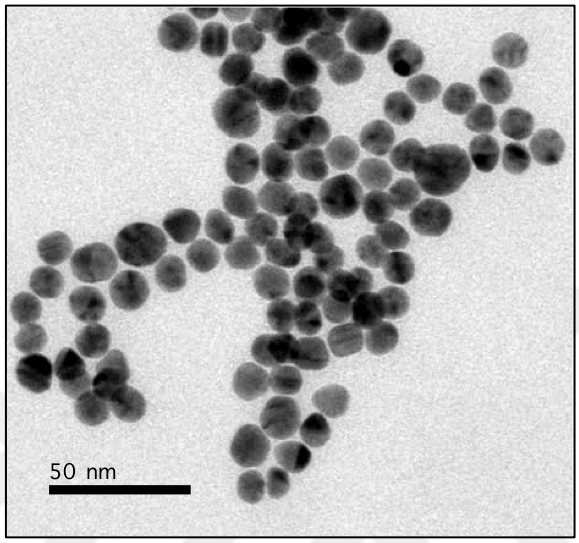

Figure 4.2. TEM image of 13 nm citrate reduced-AuNPs.

4.2. CHARACTERIZATION OF OLIGONUCLEOTIDE-FUNCTIONALIZED GOLD NANOPARTICLES

After the surface modification of AuNPs using G10 and G20 polyguanine sequences, UV/Vis spectroscopy and DLS were used for the nanoparticle (NP) characterization. According to UV-Visible spectra of polyguanine-modified AuNPs (G10-AuNPs and G20-AuNPs), maximum absorption of surface-modified NPs showed 4 nm band shifts to longer wavelength when compared to unmodified citrate-reduced AuNPs (Figure 4.3A). G10-AuNPs and G20-AuNPs showed an average hydrodynamic size of 26 nm and 32 nm, respectively (Figure 4.3B).

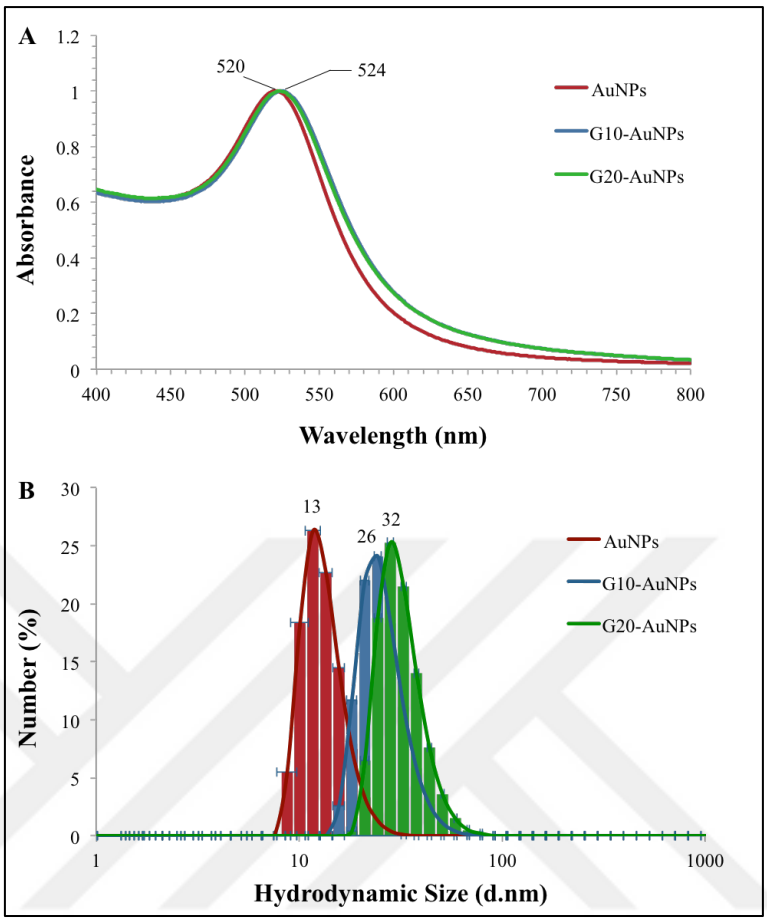

Figure 4.3. Characterization of Oligo-AuNPs. (A) UV/Visible spectra of unmodified AuNPs and polyguanine-modified AuNPs (G10-AuNPs: polyadenine-tailed G10 sequence, G20: polyadenine-tailed G20 sequence), (B) DLS data showing average hydrodynamic size of AuNPs, G10-AuNPs, and G20-AuNPs.

The surface charge of unmodified AuNPs and polyguanine-modified AuNPs was evaluated by measuring their ζ-potentials using Malvern ZetaSizer Nano ZS (Figure 4.4). Citrate-reduced AuNPs, having negative surface charge, exhibit increased surface negativity when modified with two different polyguanine sequences. The colloidal suspension of G10-AuNPs and G20-AuNPs showed an average surface charge of -34.1 and -37.6 mV, respectively.

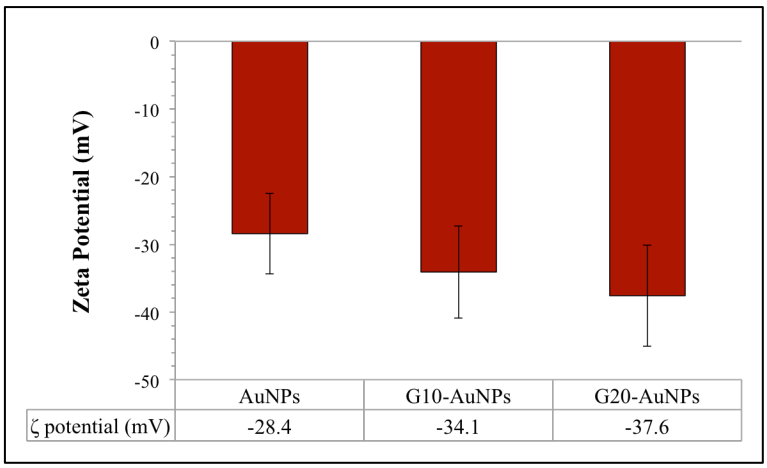

Figure 4.4. Zeta potential measurements of unmodified AuNPs, G10-AuNPs and G20-AuNPs. Data were obtained from three separate experiments ± standard deviations.

The surface modified-AuNPs were dispersed in 1X PBS, after three centrifugation steps, in order to remove the unbound oligonucleotides from the colloidal suspensions. UV/Vis spectroscopy and DLS measurements were used to evaluate λmax, average hydrodynamic size, polydispersity index (PDI), and surface charge of the NPs before and after centrifugation (Table 4.1). Maximum absorption of G10-AuNPs and G20-AuNPs did not show any band shift, and average hydrodynamic size of surface-modified AuNPs did not change, however, according to ζ-potential measurements, average surface charges of G10-AuNPs and G20-AuNPs were observed as -24.4 and -30.1 mV, respectively.

The resulting purified G10-AuNPs and G20-AuNPs were also dispersed in the cell culture medium in order to evaluate their physicochemical characteristics after incubation inside an environment consisting of serum proteins, glucose, sodium pyruvate, antibiotics, etc. (Table 4.1). When the surface-modified AuNPs were dispersed in cell culture medium including FBS, their maximum absorption slightly shifted to longer wavelengths, and DLS data showed increased average hydrodynamic sizes, 59.14 nm for G10-AuNPs, and 64.79 nm for G20-AuNPs with an increased polydispersity. Moreover, according to ζ-potential measurements, surface charges of G10-AuNPs and G20-AuNPs exhibited much more positive values such as -12.5 and -12.6 mV, respectively.

When unmodified, citrate-reduced 13 nm AuNPs were dispersed in cell culture medium, maximum absorption band, which was centered at 520 nm, were also shifted to 531 nm,

with an average hydrodynamic size of 34.95 nm. The surface charge of AuNPs was also changed to -12.8 mV from -28.4 nm.

Table 4.1. Characterization of AuNPs, G10-AuNPs and G20-AuNPs.

	UV	**DLS**		
		Size		**Surface Charge**
	λmax (nm)	**d.nm**	**PDI**	**ζ-Potential (mV)**
AuNPs	520	13.29±3.36	0.218	-28.4±5.95
G10-AuNPs	524	26.12±7.32	0.299	-34.1±6.80
G20-AuNPs	524	32.06±8.62	0.298	-37.6±7.47
G10-AuNPs$_a$	524	26.44±8.18	0.373	-24.4±9.14
G20-AuNPs$_a$	525	32.89±13.64	0.275	-30.1±9.51
AuNPs$_b$	531	34.95±7.24	0.433	-12.8±10.1
G10-AuNPs$_b$	528	59.14±3.96	0.423	-12.5±4.03
G20-AuNPs$_b$	531	64.79±1.33	0.426	-12.6±5.26

a: after centrifugation, when samples were dispersed in 1X PBS, *b*: samples dispersed in culture medium

4.3. *IN VITRO* CYTOTOXICITY OF OLIGONUCLEOTIDE-FUNCTIONALIZED GOLD NANOPARTICLES ON TUMOR CELLS AND NORMAL CELLS

U373 and U87MG cells were incubated with six different concentrations of AuNPs, G10-AuNPs, and G20-AuNPs, ranging from 0.1 to 5 nM for 24 hours and cell viability was evaluated via WST-1 cell proliferation assay (Figure 4.5). The AuNPs did not show any significant decrease in cell viability of both U373 and U87MG cells until the highest concentration of 5 nM, cell viability was reduced to 72.49 in U373 cells and 75.33 in U87MG cells (Figure 4.5A). On the other hand, G10-AuNPs and G20-AuNPs affected cell viability of U373 and U87MG cells at the concentrations of 2.5 nM and 5 nM. Cell viability of 5 nM G10-AuNPs treated cells was reduced to 69.59 in U373 cells, whereas 72.32 in U87MG cells (Figure 4.5B). Cell viability of 2.5 nM and 5 nM G20-AuNPs treated cells was reduced to 79.98 and 68.43 in U373 cells, respectively, whereas 76.89

and 71.11 in U87MG cells, respectively (Figure 4.5C). Since no significant reduction in cell viability was observed at AuNPs and Oligo-AuNPs concentrations higher than 2.5 nM, this dose of treatment was chosen for further cell viability assessments.

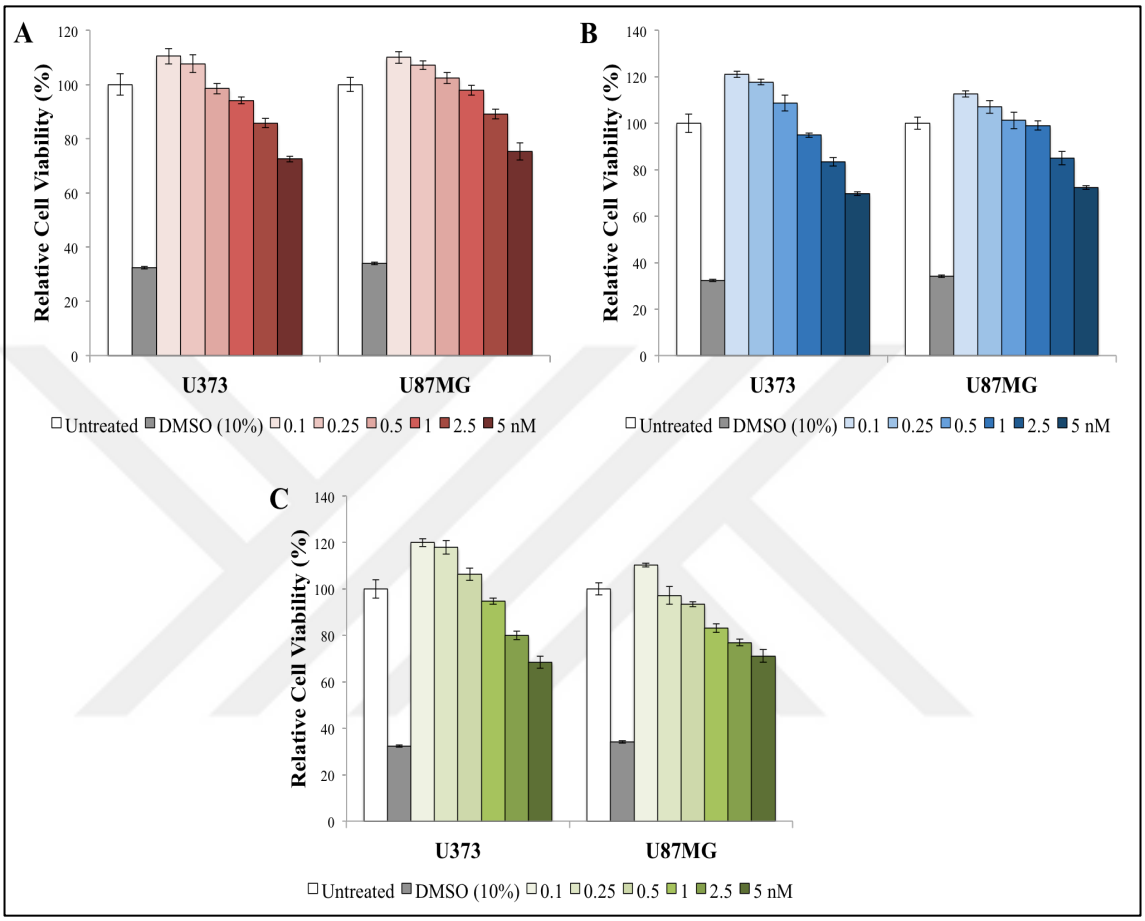

Figure 4.5. Cell viability of U373 and U87MG cells after 24 h incubations of different NP concentrations. (A) AuNPs, (B) G10-AuNPs, and (C) G20-AuNPs. DMSO (10 per cent) was used as a positive control. Data were obtained from three separate experiments ± standard deviations.

In addition to U373 and U87MG cells, NHA were also incubated with 2.5 nM AuNPs, G10-AuNPs, and G20-AuNPs for 24 hours. Relative cell viability of NHA, U373 and U87MG cells were shown in Figure 4.6. No significant reduction of cell viability was seen in NHA when cells were treated with 2.5 nM AuNPs, G10-AuNPs and G20-AuNPs for 24 hours.

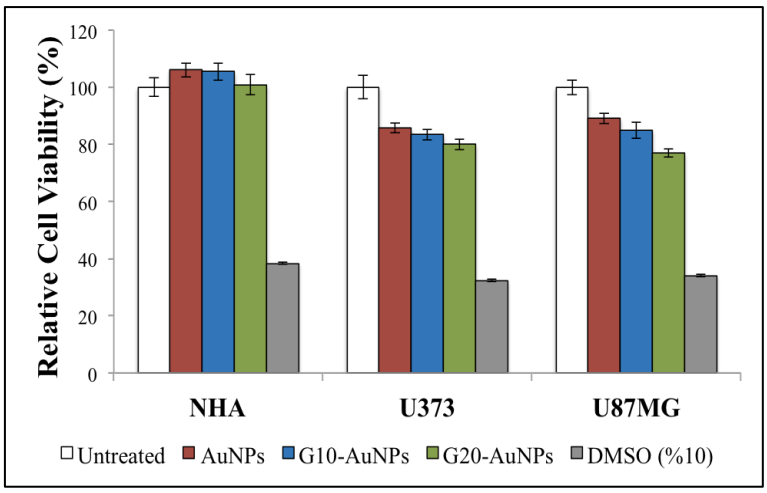

Figure 4.6. Cell viability of NHA, U373 and U87MG cells after 24 h incubations of 2.5 nM NPs. DMSO (10 per cent) was used as a positive control. Data were obtained from three separate experiments ± standard deviations.

For further cell viability assessments, NHA, U373 and U87MG cells were treated with 2.5 nM AuNPs, G10-AuNPs and G20-AuNPs up to 72 hours. Three days of incubation with 2.5 nM AuNPs showed reduced cell viability in NHA, where incubations with 2.5 nM G10-AuNPs and G20-AuNPs did not exhibit this reduction in cell viability (Figure 4.7A). U373 cells showed similar cell viability reduction for three days of incubations with G10-AuNPs and G20-AuNPs, where incubation with unmodified AuNPs did not show any significant reduction in cell viability (Figure 4.7B). On the other hand, both AuNPs and G10-AuNPs showed similar reduction in cell viability in U87MG cells when cells, where G20-AuNPs significantly affected cell viability when compared with AuNPs and G10-AuNPs (Figure 4.7C). As a result, polyguanine-modified AuNPs affected cell viability of GBM cells, where reducing harm to normal cells when compared with unmodified AuNPs.

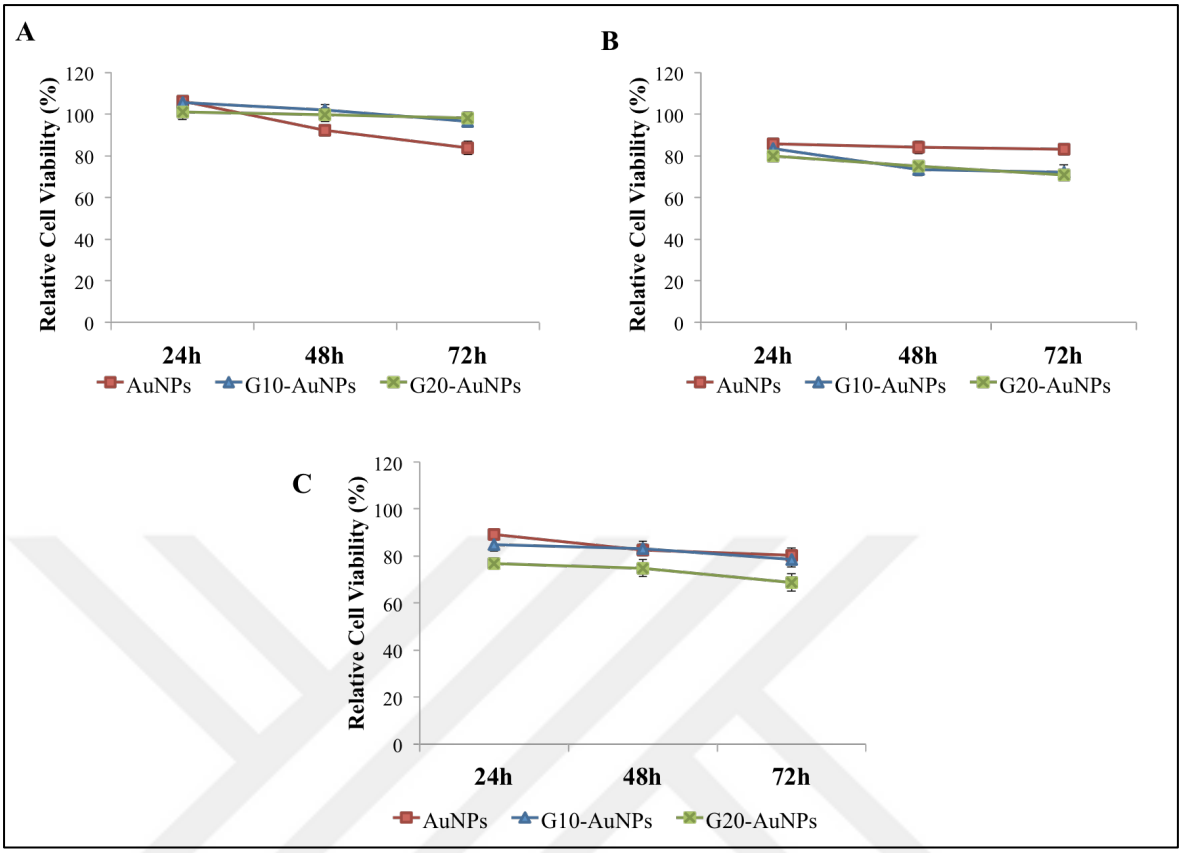

Figure 4.7. Cell viability for three days of incubations with 2.5 nM AuNPs, G10-AuNPs, and G20-AuNPs. (A) NHA, (B) U373, and (C) U87MG cells. Data were obtained from three separate experiments ± standard deviations.

Cell viability of GBM cells after three days of incubation with 2.5 nM G10-AuNPs and G20-AuNPs was also compared to the normal cells in order to examine length-dependent cellular viability, and its selective effect in normal and GBM cells (Figure 4.8). According to results, both G10-AuNPs (Figure 4.8A) and G20-AuNPs (Figure 4.8B) significantly reduced cell viability for all three days of incubations when compared to NHA. Moreover, G20-AuNPs affected the cellular viability more significantly than G10-AuNPs in both GBM cell lines.

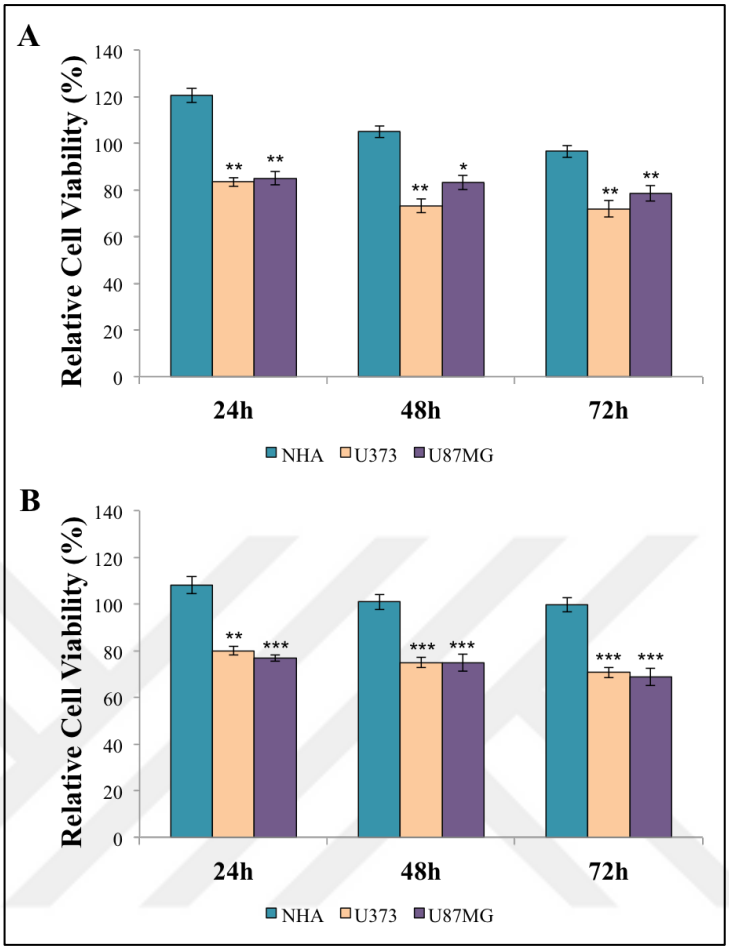

Figure 4.8. Cell viability of NHA, U373 and U87MG cells after three days of incubations with NPs. (A) 2.5 nM G10-AuNPs, and (B) 2.5 nM G20-AuNPs. Data were obtained from three separate experiments ± standard deviations. Treated cells were compared with NHA cells using a paired two-tailed Student's t test. A p-value < 0.05 was considered as a significance level, and the data were labeled with * for $p < 0.05$, ** for $p < 0.01$, and *** for $p < 0.001$, respectively.

4.4. DETECTION OF THE CELL CYCLE DISTRIBUTION OF OLIGONUCLEOTIDE-FUNCTIONALIZED GOLD NANOPARTICLES

Cell cycle analysis was performed to evaluate the distribution of cell populations in G_0/G_1, S and G_2/M phase following 24 h treatment of AuNPs, G10-AuNPs and G20-AuNPs. While there were no significant changes in cell distribution in NHA after NP treatments (Figure 4.9A), surface modified-AuNPs with G10 and G20 polyguanine sequences showed

increased S and G_2/M phase arrest in U373 and U87MG cells (Figure 4.9B and Figure 4.9C).

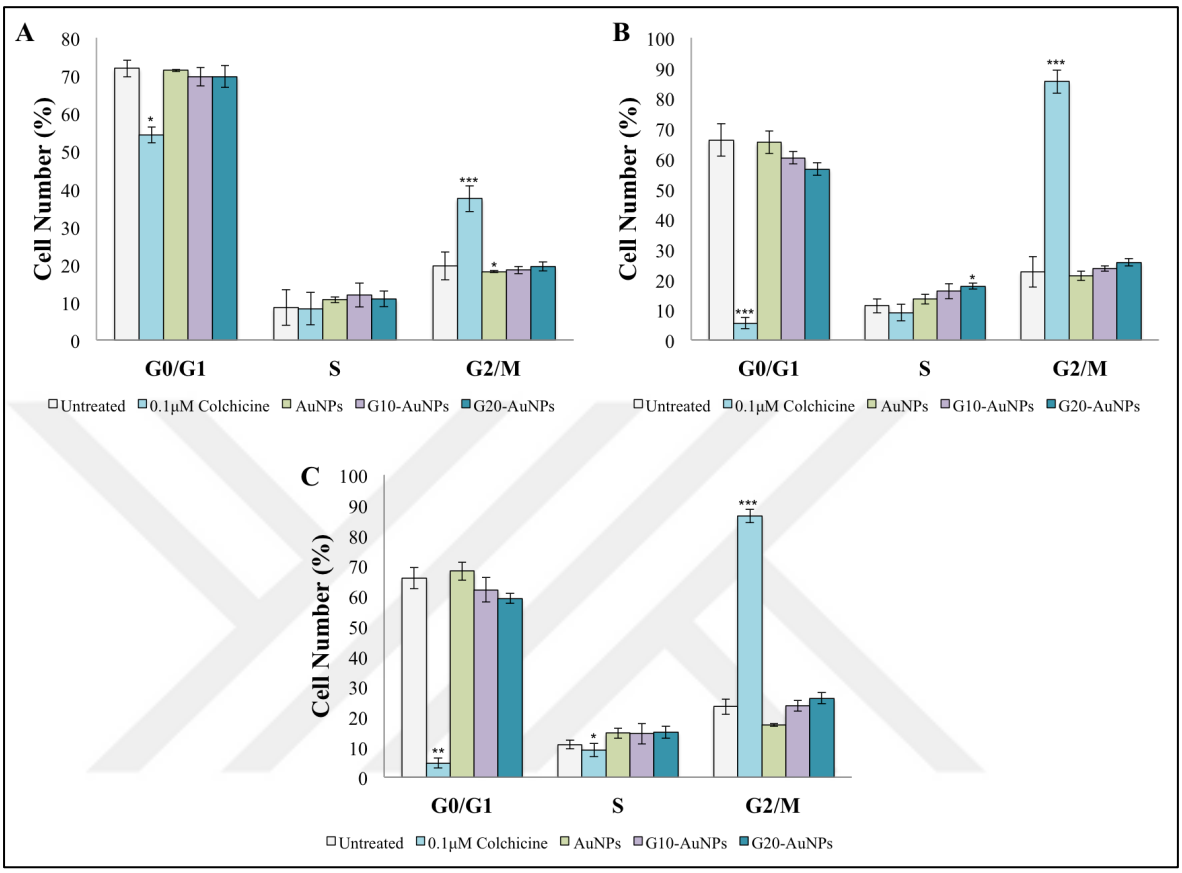

Figure 4.9. Cell cycle analysis following a 24 h treatment period with 2.5 nM AuNPs, G10-AuNPs and G20-AuNPs. (A) NHA, (B) U373, and (C) U87MG cells. As a control, cells were also treated with 0.1 µM colchicine to arrest the cells at G_2/M phase. Data were obtained from three separate experiments ± standard deviations. Treated cells were compared with control cells using a paired two-tailed Student's t test. A p-value < 0.05 was considered as a significance level, and the data were labeled with * for $p < 0.05$, ** for $p < 0.01$, and *** for $p < 0.001$, respectively.

To determine the alterations of cell cycle arrests in GBM and normal cells, distribution of cells in different phases of cell cycle were compared with normal cells after 24 hours of treatment with 2.5 nM G10-AuNPs and G20-AuNPs (Figure 4.10). Treatment of U373 and U87MG cells with 2.5 nM G10-AuNPs for 24 h resulted a significant accumulation of cells in G_2/M phase when compared to normal cells (Figure 4.10A). Additionally, the treatment with 2.5 nM G20-AuNPs for 24 h significantly affected GBM cells, and resulted cell

accumulations in both S phase and G_2/M phase (Figure 4.10B). In U373 cells, it is clearly seen that G20-AuNPs significantly arrested cells in S and G_2/M phase, while significantly reduced cell accumulation in G_0/G_1.

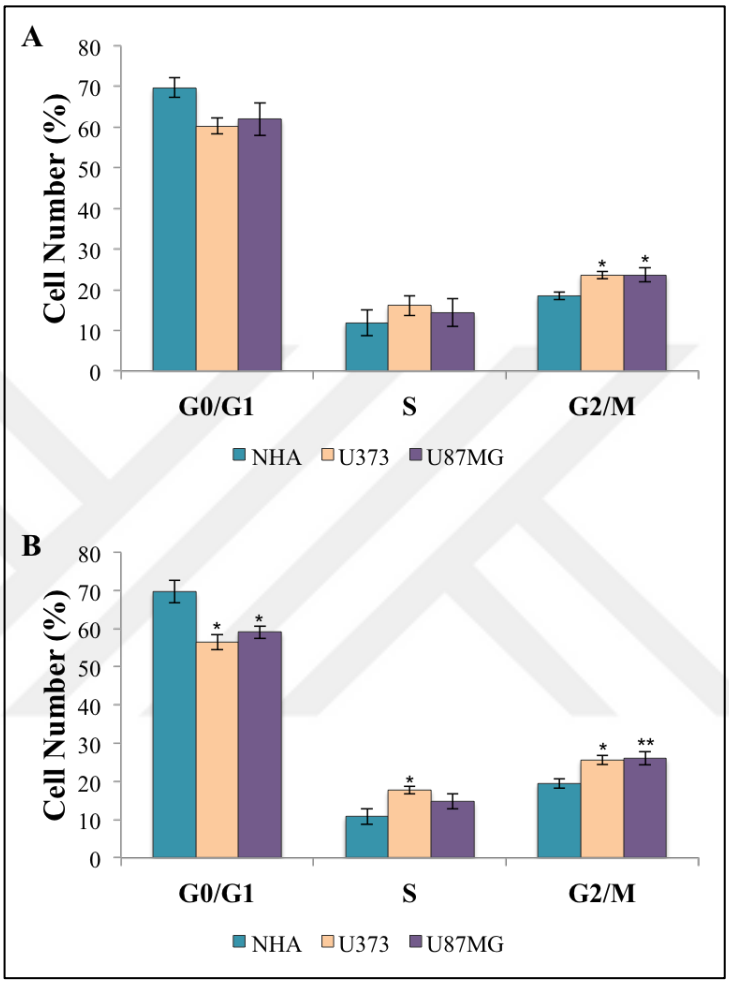

Figure 4.10. Cell cycle analysis of NHA, U373 and U87MG cells following a 24 h treatment period with NPs. (A) 2.5 nM G10-AuNPs, and (B) 2.5 nM G20-AuNPs. Data were obtained from three separate experiments ± standard deviations. Treated cells were compared with NHA cells using a paired two-tailed Student's t test. A p-value < 0.05 was considered as a significance level, and the data were labeled with * for $p < 0.05$, and ** for $p < 0.01$, respectively.

Fold increase in cell accumulations in both S and G_2/M phase in cell cycle analysis were seen in Table 4.2. Treated cells were compared with both GBM control cells and NHA, and according to results, it was found that G20-AuNPs arrested cells in S phase in U373 (1.57 fold increase), where U87MG cells did not show that much significant progression in

S phase. On the other hand, when cell distribution of polyguanine-modified treated GBM cells were compared with normal cells, it was revealed that G20-AuNPs increased cell population in both S and G_2/M phase while the highest cell accumulation in S phase was seen in U373 cells, with a 1.64 fold increase. In addition, in U87MG cells G20-AuNPs arrested cells in G_2/M phase with a 1.34-fold increase when compared to healthy cells (Table 4.2).

Table 4.2. Fold increase of S and G_2M phase in cell cycle analysis.

	Fold Increase			
	G10-AuNPs		**G20-AuNPs**	
	S	**G_2/M**	**S**	**G_2/M**
U373$_a$	1.42	1.05	1.57*	1.14
U87MG$_a$	1.33	1.01	1.37	1.12
U373$_b$	1.36	1.28†	1.64†	1.32†
U87MG$_b$	1.21	1.28†	1.36	1.34††

Data were obtained from three separate experiments ± standard deviations. Treated cells were compared with *a*: control cells and *b*: NHA, using a paired two-tailed Student's t test. A p-value < 0.05 was considered as a significance level for both analysis, and the data were labeled with * for $p < 0.05$ (Group *a*), † for $p < 0.05$ and †† for $p < 0.01$ (Group *b*), respectively.

4.5. CELLULAR UPTAKE STUDIES AND NANOPARTICLE CALCULATIONS

Cellular uptake studies were performed via UV/Vis spectroscopic measurements of NPs prepared in phenol red-free media. NHA, U373 and U87MG cells were used for 24 h cellular uptake studies of 2.5 nM G10-AuNPs and G20-AuNPs, and number of nanoparticles per cells were shown in Table 4.3. The concentrations of G10-AuNPs and G20-AuNPs were first determined by UV/Vis measurements, and then converted to the number of G10-AuNPs and G20-AuNPs per cell using the number of cells in each well.

Table 4.3. Average number of polyguanine-modified AuNPs taken up per NHA, U373 and U87MG cells.

***N* (x10^5/ cell)** / **Cells**	**G10-AuNPs**	**G20-AuNPs**
NHA	1.50±0.04	2.01±0.10
U373	1.88±0.15	3.12±0.21
U87MG	2.06±0.07	3.73±0.41

Data were obtained from three separate experiments ± standard deviations. *N* is the number of NPs taken up per cell.

Quantification of NP uptake by NHA, U373 and U87MG were seen in Figure 4.11, and results were compared with NPs, and between GBM cells and normal cells. According to results, cellular uptake of G20-AuNPs was higher than G10-AuNPs for all three cell lines. When G20-AuNPs and G10-AuNPs were compared, the fold-increases in number of nanoparticles taken up per cell were 1.34, 1.81, and 1.66 for NHA, U373 and U87MG, respectively. Additionally, for cellular uptake of G20-AuNPs by GBM cells, results were compared with NHA, and it was found that number of nanoparticles taken up per cells were increased in 1.55-fold and 1.86-fold, in U373 and U87MG cells, respectively. The highest uptake was calculated as 3.7x10^5 G20-AuNPs per cell (U87MG).

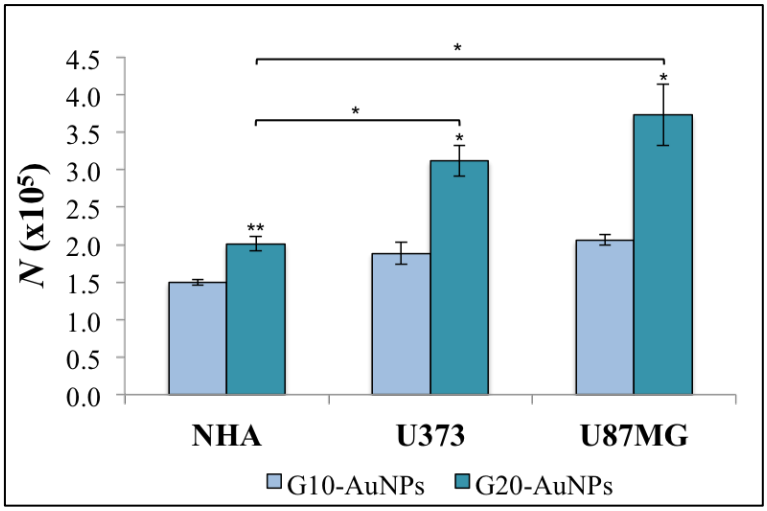

Figure 4.11. Quantification of nanoparticle uptake by NHA, U373 and U87MG cells following a 24 h-treatment period with 2.5 nM G10-AuNPs and G20-AuNPs. (*N* represents nanoparticles per cell). Data were obtained from three separate experiments ± standard deviations. Treated cells were compared with control cells using a paired two-tailed Student's t test. A p-value < 0.05 was considered as a significance level, and the data were labeled with * for $p < 0.05$, and ** for $p < 0.01$, respectively.

The relationship between cell viability and cellular uptake of NHA, U373 and U87MG cells after 24 h of incubations with G10-AuNPs and G20-AuNPs were seen in Figure 4.12. Cell viability was decreased with increased NP uptake per cell. Additionally, G20-AuNPs entered cells in much higher numbers, and showed much more reduced cell viability. Finally, GBM cells when compared to NHA showed reduced cell viability and enhanced cellular uptake for both polyguanine-modified AuNPs.

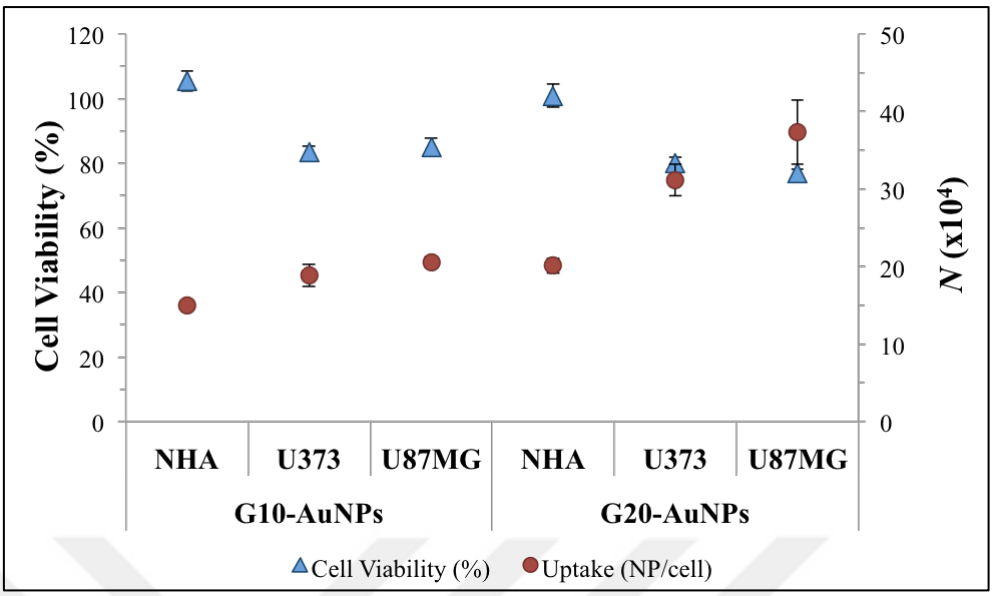

Figure 4.12. Relationship between cell viability and cellular uptake (Nx10^4) of NHA, U373 and U87MG cells after 24 h treatment of G10-AuNPs and G20-AuNPs. Data were obtained from three separate experiments ± standard deviations.

4.6. DETECTION OF APOPTOTIC CELLS

The distribution of cells in early and late apoptosis, and necrosis was detected by using Annexin V Early Detection kit (Figure 4.13). Cells scored as healthy, live cells (Annexin V-/PI-), early apoptotic (Annexin V+/PI-), late apoptotic and necrotic cells (Annexin V+/PI+). Concentration at 2.5 nM of G10-AuNPs and G20-AuNPs did not induce apoptosis in NHA (Figure 4.13A), whereas in U373 and U87MG cells, G10-AuNPs and G20-AuNPs induced early and late apoptosis. According to results, G10-AuNPs and G20-AuNPs showed 2.4 and four-fold increase in early apoptosis in U373 cells, respectively (Figure 4.13B). Moreover, G10-AuNPs and G20-AuNPs showed two and three-fold increase in early apoptosis in U87MG cells, respectively (Figure 4.13C).

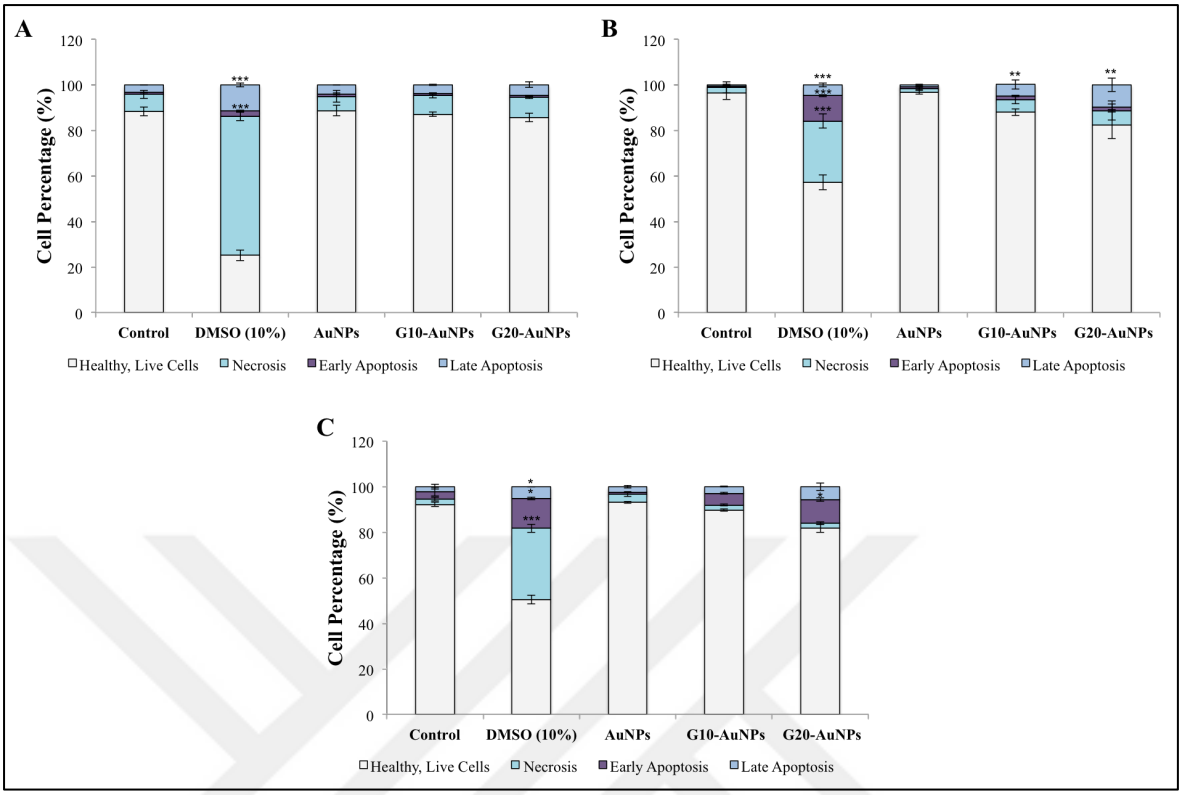

Figure 4.13. Flow cytometric analysis following a 24 h treatment period with 2.5 nM AuNPs, G10-AuNPs and G20-AuNPs. (A) NHA, (B) U373, and (C) U87MG cells. As a control, cells were treated with DMSO 10 per cent to induce apoptosis in cells. Data were obtained from three separate experiments ± standard deviations. Treated cells were compared with control cells using a paired two-tailed Student's t test. A p-value < 0.05 was considered as a significance level, and the data were labeled with * for $p < 0.05$, ** for $p < 0.01$, and *** for $p < 0.001$, respectively.

Apoptosis induction by 24-hour treatment of 2.5 nM AuNPs, G10-AuNPs and G20-AuNPs was quantified using flow cytometry (Figure 4.14). According to results, polyguanine-modified AuNPs did not induce apoptosis in NHA, while unmodified AuNPs did. On the other hand, G10-AuNPs and G20-AuNPs induced apoptosis in U373 and U87MG cells. Apoptosis induction using G10-AuNPs showed five and three per cent increase in U373 cells and U87MG cells, respectively whereas apoptosis induction of G20-AuNPs showed 10 per cent increase in both U373 and U87MG cells. The difference in quantification apoptosis induction of G20-AuNPs and G10-AuNPs revealed two fold increase in both cell lines when cells were treated with G20-AuNPs.

When apoptosis induction was compared between NHA and cancerous cells, it was revealed that for both GBM cell lines, 24-hour treatment with G20-AuNPs showed significant increase, while unmodified AuNPs showed decreased apoptotic cells population (Figure 4.14).

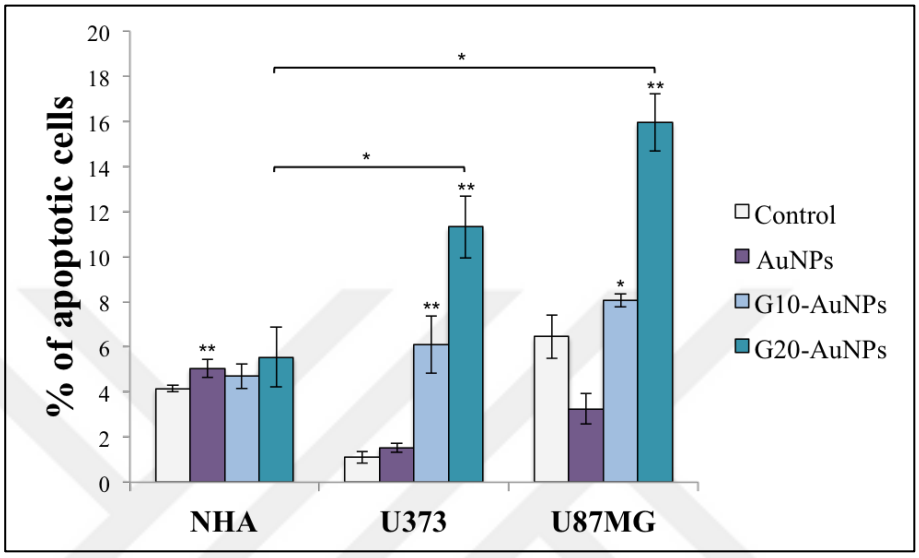

Figure 4.14. Quantification of apoptosis induction of NHA, U373 and U87MG cells following a 24 h treatment period with 2.5 nM AuNPs, G10-AuNPs and G20-AuNPs. Data were obtained from three separate experiments ± standard deviations. Treated cells were compared with control cells and GBM cells were compared with NHA using a paired two-tailed Student's t test. A p-value < 0.05 was considered as a significance level, and the data were labeled with * for $p < 0.05$, and ** for $p < 0.01$, respectively.

The relationship between apoptosis and cellular uptake of NHA, U373 and U87MG cells after 24 h of incubations with G10-AuNPs and G20-AuNPs were seen in Figure 4.15. Cellular uptake was directly proportional to apoptosis induction in all cell lines. Additionally, G20-AuNPs entered cells in higher numbers, and showed more induced apoptosis in GBM cells, while normal cells did not exhibit this apoptosis induction despite the number of polyguanine-modified AuNPs taken up per cells.

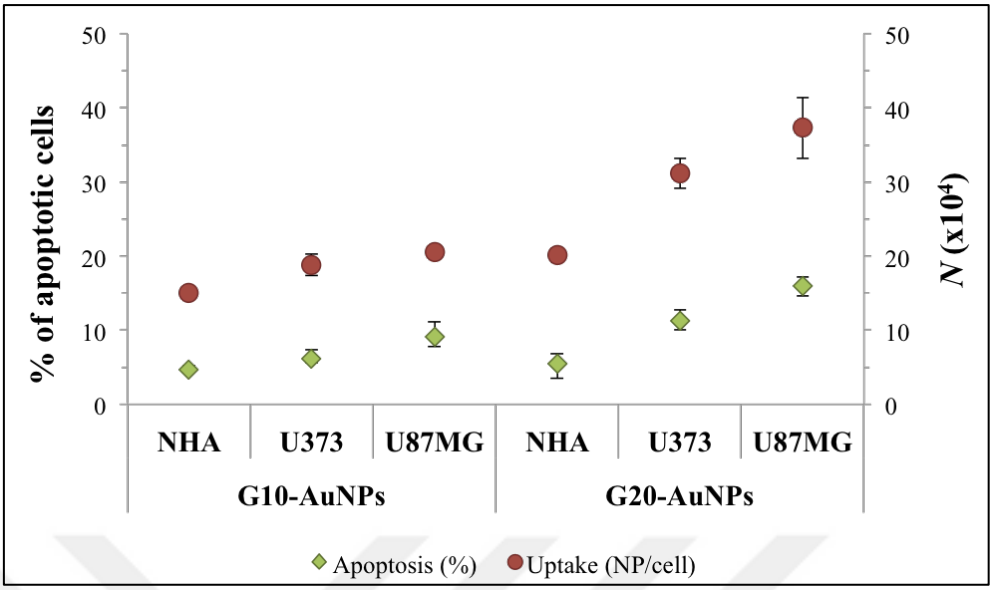

Figure 4.15. Relationship between apoptosis induction and cellular uptake (Nx10^4) of NHA, U373 and U87MG cells after 24 h treatment of G10-AuNPs and G20-AuNPs. Data were obtained from three separate experiments ± standard deviations.

5. DISCUSSION

Therapeutic nanomedicine focuses on using AuNPs as a potential agent for various reasons. First, AuNPs are inert nanomaterials and they are considered as biocompatible as a consensus. Second, AuNPs have extraordinary physical, chemical, and optical properties resulting mostly because of being plasmonic [4, 5]. Finally, synthesis and surface functionalization of AuNPs are easy compared to other nanoparticles, and their resulted colloidal suspension contains mostly monodispersed nanoparticles [3, 24]. AuNPs and surface modified-AuNPs have been investigated as delivery, and targeting agent, as well as imaging agent in nanomedicine [6, 178-180].

The surface of AuNPs can be modified using various biomolecules, and one of the most crucial biological molecules that are widely investigated in nanomedicine is oligonucleotide. Oligonucleotides can be delivered into cells efficiently when attached on the surface of AuNPs by alkyl thiol adsorption [51]. Among all nucleic acids, delivery of G-rich oligonucleotides into cells gain interest due to their anti-proliferative effects, and their unique formation allows the facilitated entry through the cellular membrane. Moreover, monomeric guanine sequences also studied, and G15 demonstrated as a promising agent [107, 108].

In addition, the chemistry on the surface of AuNPs can have significant effect on the cellular response such as increased uptake and induced apoptosis, reduced viability, and alterations of cell cycle that lead to cellular arrest in different phases [49, 78, 106]. By using polyguanine sequences that differ only in length, length-dependent cellular responses were investigated in NHA, U373 and U87MG cell lines to understand how slight change in guanine base number can affect cellular viability, uptake, apoptosis, and cell cycle. As a number of guanine bases, 10 and 20 homopolymeric guanine bases were chosen and sequences were synthesized with a polyadenine tail consisting of 10 adenine bases, that acts as a spacer, and with a thiol end, that provide S-Au binding [59].

As a functionalization method, fast salt aging was preferred because when optimized SDS amount, and phosphate buffer was used DNA loading was achieved maximized on the surface of AuNPs [172]. After the surface modification of 13 nm AuNPs, modified-nanoparticles were characterized by using DLS, and UV/Vis spectroscopy (Figure 4.3). Surface-modified AuNPs exhibited SPR band shift to higher wavelegth and displaying

higher average hydrodynamic size demostrating the successful functionalization. G20-AuNPs had higher hydrodynamic size than G10-AuNPs, which was expected because of increased number of bases in oligonucleotide sequences (Figure 4.3B). Moreover, surface charge of the modified AuNPs were evaluated by measuring their ζ-potentials, and exhibited increase negativity on the surface of AuNPs when modified with polyguanine sequences, and also G20-AuNPs showed more negative surface charge than G10-AuNPs, which was expected due to increased number of bases, more negative charge resulted from increased number phosphate groups of the DNA backbone [181].

The characterization of polyguanine-modified AuNPs after the centrifugation and when dispersed in cell culture medium were also performed to examine their behavior in different environments such as PBS, or media consisting serum proteins (Table 4.1). The unmodified AuNPs were fully aggregated when dispersed in PBS because after centrifugation the steric repulsion due to citrate adsorption on AuNPs surface was also disappeared, which resulted in aggregation of AuNPs [182]. However, when the surface of AuNPs was modified, NPs continue their dispersion in a colloidal form. After centrifugation, the unbound oligonucleotides were removed from the colloidal suspension and G10-AuNPs and G20-AuNPs showed similar band shift, surface charge and their hydrodynamic sizes were not affected significantly, suggesting a successful and stable surface functionalization.

When G10-AuNPs and G20-AuNPs dispersed in cell culture medium, NPs aggregated due to adsorbed serum proteins on the surface of AuNPs and showed higher average hydrodynamic size and SPR band shift to higher wavelength (Table 4.1). The length of the oligonucleotide sequence affected the aggregation, and G20-AuNPs showed higher values of maximum absorption with a higher average hydrodynamic size than G10-AuNPs. Surface charge also affected from serum adsorption, and the effect was also length-dependent [64]. The unmodified AuNPs and surface modified AuNPs exhibited much more positive surface charges because of the serum proteins adsorbed on surface, and DNA loading also affected serum adsorption. Hence, serum adsorption was higher when G20-AuNPs were considered, and it can be seen from surface charges (Table 4.1).

After the evaluation of physicochemical characteristics of NPs used in this study, cellular experiments were performed systematically. For cellular assessments, NHA, U373 and U87MG cells were chosen. U373 and U87MG cancerous cell lines and NHA cells were

preferred to investigate changes in cellular responses between astrocytes and GBM after cells were treated with G-rich polyguanine-modified AuNPs. According to several studies, G-rich sequences were known to recognize and bind to nucleolin, which were highly expressed in cancer cells including GBM [76, 102]. Recent studies also showed that nucleolin that was expressed on the surface of phagocytes possessed SR-like activity, and it was also known that poly-G sequences were a natural ligands also for SR-A [183, 184]. The recognition of nucleolin provide increased uptake of G-rich sequences inside of these cancerous cells, which could also affect biological response [64, 169, 185]. Moreover, monomeric G-oligonucleotide, 20 bases in length were demonstrated to induced apoptosis and altered cell cycle progression in tumor cells, and reduced harm to normal cells [78]. Hence, comparison between healthy and cancerous cells would provide crucial knowledge about cancer therapy.

Cell viability of U373 and U87MG cells, which were incubated with various concentrations, from 0.1 nM to five nM, of AuNPs, G10-AuNPs and G20-AuNPs for 24 hours, revealed that 2.5 nM could be chosen as a dose of treatment for further treatments because no significant reduction in cellular viability was observed concentration higher than the chosen one (Figure 4.5). After determination of the concentration, this dose of treatment was also used for cell viability evaluation of NHA to compare between normal and cancerous cells (Figure 4.6). Results demonstrated that dose of treatment was significantly affected cancerous cells while reducing harm to normal cells.

After the determination of treatment concentration for NHA, and GBM cells, cellular viability was observed upto three days of incubations with NPs to evaluate their lasting cell viability effects upto 72 hours. Three-day evaluation of cell viability showed significant reduction when GBM cells treated with G10-AuNPs and G20-AuNPs, however NHA did not affected this much of reduction, while unmodified AuNPs reduced the cell viability (Figure 4.7). Results demostrated that dose of treatment of polyguanine-modified AuNPs with increased treatment days significantly affect cancerous cells while normal cells did not affected, demonstrating the retention of NPs inside of the cells or cell-associated state for at least three days. Moreover, when affected cellular viability of G10-AuNPs and G20-AuNPs treated GBM cells were compared with normal cells, results suggested both length-dependent and selective toxicity in GBM cells (Figure 4.8).

After the evaluation of cell viability with an effective concentration, 24 hours of treatments with AuNPs, G10-AuNPs, and G20-AuNPs were performed to analyze cell cycle distribution using flow cytometer. Cell cycle analysis showed an arrest in S and G_2/M phase when GBM cells were treated with 2.5 nM polyguanine-modified AuNPs for 24 hours (Figure 4.9), while normal cells were not affected significantly, demonstrating a selective cell cycle progression. Additionally, when phase accumulations of GBM cells treated with polyguanine-modified AuNPs were compared with normal cells, results showed significant arrests in both S and G_2/M phase, with a length-dependent increase suggesting that guanine base number significantly affected phase distributions, in addition to previous studies demonstrating effects of G-rich oligonucleotides in cell cycle progression in tumor cells [78, 99]. The highest cell accumulation was seen in S phase when U373 cells were treated with G20-AuNPs, demonstrating a selective cell accumulation in S phase was seen when GBM cells were treated with G20-AuNPs (Table 4.2).

Prior to quantification of apoptosis induction of polyguanine-modified AuNPs, G10-AuNPs and G20-AuNPs were used for cellular uptake studies using a simple spectroscopic method, UV/Vis spectroscopy, to calculate the number of nanoparticles engulfed by cells, or associated with cells. The unmodified AuNPs were not suitable for this experiment because they showed aggregation in medium after 24 hours incubation with cells, which would interfere with UV/Vis spectroscopic measurements for uptake studies [186]. The method was based on the dispersion of desired concentration of nanoparticles in phenol-red free media before any incubation with cells because SPR band of phenol red would overlap with absorbance peaks of G10-AuNPs and G20-AuNPs [174], and phenol red-free media was used as a blank prior to other UV/Vis measurements. The absorbance difference of media before and after incubations were considered as NPs taken up or surface-associated by cells because loosely-bound NPs on the surface of cell membrane were washed off by three PBS washing steps [174]. Absorbance differences were used for NP concentrations, which were taken up or surface-associated by cells using Beer's Law [143, 170, 172], and additionally, by using the literature knowledge the average number of NPs taken up by cells were calculated [22, 176]. According to results, cellular uptake was highest when U87MG cells were treated with G20-AuNPs for 24 hours (Table 4.3 and Figure 4.11). Moreover, G10-AuNPs showed similar cellular uptake for NHA, U373 and U87MG cells,

where NHA was the lowest but not significantly. In addition, cellular uptake of G20-AuNPs was higher than G10-AuNPs for all cell lines while cancerous cells interacted with significantly higher number of G20-AuNPs than normal cells, which could be the result of the highly expressed nucleolin receptor on the surface of GBM cells responsible for G-rich oligonucleotide uptake [76, 102]. Cell cycle results revealed the highest uptake calculated as $3.7x10^5$ G20-AuNPs per cell for U87MG, which could be resulted due to upregulation of nucleolin in U87MG, and higher expression of nucleolin on the surface of U87MG than U373 [187].

Distribution of cells in early and late apoptosis, and necrosis was detected by apoptosis assay using flow cytometer (Figure 4.13). DMSO (10 per cent) was used as a positive control, and significantly induced apoptosis in GBM cells, while mostly induced necrosis in NHA. According to results, G20-AuNPs induced early apoptosis more than G10-AuNPs in U373 cells and U87MG cells, suggesting a length-dependent anti-proliferative effects and induction of apoptosis in GBM cells. It was known that GROs induced apoptosis in tumor cells [97, 98], and a recent study demonstrated 20-mer monomeric guanine selectively induced apoptosis in malignant esophageal cell line, OE19 [78]. In addition to these studies, in this study it was suggested that AuNPs could be effective nanocarriers for GRO delivery, and using two monomeric guanine sequences differ in length demonstrating a length-dependent cell cycle response in GBM cells.

Quantification of apoptosis induction by AuNPs, G10-AuNPs and G20-AuNPs were performed to compare the results between cell lines, and nanoparticles (Figure 4.14). Results demonstrated that polyguanine-modified AuNPs induced apoptosis in cancerous cells, while no induction was quantified in normal cells, except unmodified AuNPs. Unmodified AuNPs significantly induced apoptosis in normal astrocytes, while not affected GBM cells to induce any apoptosis. In addition, G10-AuNPs and G20-AuNPs significantly induced apoptosis in cancerous cells when compared with their untreated control cells and normal astrocytes, with a higher apoptosis induction when cells were treated with G20-AuNPs. The reason for that could be the enhanced cellular uptake of G20-AuNPs when compared with G10-AuNPs, and in GBM cells than normal cells.

For final remarks, relationships between cell viability and cellular uptake, cellular uptake and apoptosis induction were evaluated (Figure 4.12 and Figure 4.15), and found that viability and uptake were inversely proportional, while uptake and apoptosis were directly

proportional. G20-AuNPs significantly enhanced cellular uptake, reduced cell viability, and induced apoptosis in U373 and U87MG cells, suggesting a length-dependent selective killing of GBM cells.

6. CONCLUSION AND FUTURE PERSPECTIVE

In this study, how slight changes in surface chemistry of AuNPs could significantly change cellular responses in GBM was studied. This study demonstrated that increasing number of guanine bases enhanced cellular uptake, altered cell cycle progression and increased anti-proliferative effects and induction of apoptosis in glioblastoma (GBM) cells (U87MG and U373) while reducing harm to normal human astrocytes (NHA). The data in this study suggests length-dependent selective killing of GBM cells using polyguanine modified-AuNPs, however, a little more molecular insight is needed to understand the nature of G20-AuNPs and G10-AuNPs.

In addition to enlightening the molecular structure of monomeric polyguanine sequences, the uptake mechanism (surface receptors, endocytosis pathway), the subcellular localization (TEM, Dark-field microscopy, Confocal microscopy), and the apoptotic pathways (p53, caspase 3/7 activity) should also be investigated. This study is the first report that shows the length-dependent selective killing of polyguanine-modified AuNPs in GBM cells. Therefore, G-rich oligonucleotide modified-AuNPs can be suggested as a promising novel therapeutic agent for drug and small molecule delivery for brain tumor research.

Further studies may include preparation of *in vitro* co-culture of the human BBB for developing BBB-targeted strategies using polyguanine modified-AuNPs, which can be conjugated with small molecules and drugs, as well as coupled with targeting moieties such as antibodies. Additionally, further investigations can be directed to telomerase activity in GBM cells, or other malignant tumor types having highly expressed nucleolin on their cell surface such as breast cancer cells, when treated with BBB-permeable poly-G modified-AuNPs. Moreover, by using polyguanine modified-AuNPs gene expression can be manipulated in GBM cells, and after *in vitro* trials, *in vivo* GBM models can be used for further examine the tumor growth.

Other than cancer therapy, polyguanine-modified AuNPs can also be investigated as therapeutic agents for other neurological disorders such as Alzheimer's disease or as imaging agents. By targeting Aβ fibrils combined with photothermal therapy, AuNPs can be used to slow down the progression of Alzheimer's disease, and with polyguanine or guanine rich oligonucleotide surface modification of AuNPs can facilitate the delivery

across BBB. Finally, by targeting telomeres and telomerases, aging can also be studied in addition to therapy of cancer and other neurological disorders.

REFERENCES

1. Faraday, M., *The Bakerian lecture: experimental relations of gold (and other metals) to light.* Philosophical Transactions of the Royal Society of London, 1857. **147**: p. 145-181.

2. Turkevich, J., P.C. Stevenson, and J. Hillier, *A study of the nucleation and growth processes in the synthesis of colloidal gold.* Discussions of the Faraday Society, 1951. **11**: p. 55-75.

3. Frens, G., *Controlled nucleation for the regulation of the particle size in monodisperse gold suspensions.* Nature, 1973. **241**(105): p. 20-22.

4. Kamat, P.V., *Photophysical, photochemical and photocatalytic aspects of metal nanoparticles*. 2002, ACS Publications.

5. Kelly, K.L., et al., *The optical properties of metal nanoparticles: the influence of size, shape, and dielectric environment*. 2003, ACS Publications.

6. Sapsford, K.E., et al., *Functionalizing nanoparticles with biological molecules: developing chemistries that facilitate nanotechnology.* Chemical reviews, 2013. **113**(3): p. 1904-2074.

7. Kneipp, K., H. Kneipp, and H.G. Bohr, *Single-molecule SERS spectroscopy*, in *Surface-Enhanced Raman Scattering*. 2006, Springer. p. 261-277.

8. Kateb, B., et al., *Nanoneuroscience and Nanoneurosurgery*, in *The Textbook of Nanoneuroscience and Nanoneurosurgery*. 2013, CRC Press. p. 547-556.

9. O'Neal, D.P., et al., *Photo-thermal tumor ablation in mice using near infrared-absorbing nanoparticles.* Cancer letters, 2004. **209**(2): p. 171-176.

10. Ferrari, M., *Cancer nanotechnology: opportunities and challenges.* Nature Reviews Cancer, 2005. **5**(3): p. 161-171.

11. Davis, M.E. and D.M. Shin, *Nanoparticle therapeutics: an emerging treatment modality for cancer.* Nature reviews Drug discovery, 2008. **7**(9): p. 771-782.

12. Li, J., J. Liu, and C. Chen, *Remote Control and Modulation of Cellular Events by Plasmonic Gold Nanoparticles: Implications and Opportunities for Biomedical Applications.* ACS nano, 2017. **11**(3): p. 2403-2409.

13. El-Sayed, I.H., X. Huang, and M.A. El-Sayed, *Selective laser photo-thermal therapy of epithelial carcinoma using anti-EGFR antibody conjugated gold nanoparticles.* Cancer letters, 2006. **239**(1): p. 129-135.

14. Zhang, L., et al., *Nanoparticles in medicine: therapeutic applications and developments.* Clinical pharmacology and therapeutics, 2008. **83**(5): p. 761-769.

15. Kateb, B. and J.D. Heiss, *The textbook of nanoneuroscience and nanoneurosurgery*. 2013: CRC Press.

16. Chithrani, B.D. and W.C. Chan, *Elucidating the mechanism of cellular uptake and removal of protein-coated gold nanoparticles of different sizes and shapes.* Nano letters, 2007. **7**(6): p. 1542-1550.

17. Ma, X., et al., *Gold nanoparticles induce autophagosome accumulation through size-dependent nanoparticle uptake and lysosome impairment.* ACS nano, 2011. **5**(11): p. 8629-8639.

18. Gong, N., et al., *Effects of the physicochemical properties of gold nanostructures on cellular internalization.* Regenerative biomaterials, 2015: p. rbv024.

19. Oh, E., et al., *Cellular uptake and fate of PEGylated gold nanoparticles is dependent on both cell-penetration peptides and particle size.* Acs Nano, 2011. **5**(8): p. 6434-6448.

20. Huang, K., et al., *Size-dependent localization and penetration of ultrasmall gold nanoparticles in cancer cells, multicellular spheroids, and tumors in vivo.* ACS nano, 2012. **6**(5): p. 4483-4493.

21. De Jong, W.H., et al., *Particle size-dependent organ distribution of gold nanoparticles after intravenous administration.* Biomaterials, 2008. **29**(12): p. 1912-1919.

22. Chithrani, B.D., A.A. Ghazani, and W.C. Chan, *Determining the size and shape dependence of gold nanoparticle uptake into mammalian cells.* Nano letters, 2006. **6**(4): p. 662-668.

23. Albanese, A. and W.C. Chan, *Effect of gold nanoparticle aggregation on cell uptake and toxicity.* ACS nano, 2011. **5**(7): p. 5478-5489.

24. Perrault, S.D. and W.C. Chan, *Synthesis and surface modification of highly monodispersed, spherical gold nanoparticles of 50− 200 nm.* Journal of the American Chemical Society, 2009. **131**(47): p. 17042-17043.

25. Kimling, J., et al., *Turkevich method for gold nanoparticle synthesis revisited.* The Journal of Physical Chemistry B, 2006. **110**(32): p. 15700-15707.

26. Wu, H.-Y., et al., *Seed-mediated synthesis of high aspect ratio gold nanorods with nitric acid.* Chemistry of materials, 2005. **17**(25): p. 6447-6451.

27. Pérez-Juste, J., et al., *Gold nanorods: synthesis, characterization and applications.* Coordination Chemistry Reviews, 2005. **249**(17): p. 1870-1901.

28. Skrabalak, S.E., et al., *Gold nanocages: synthesis, properties, and applications.* Accounts of chemical research, 2008. **41**(12): p. 1587-1595.

29. Chen, J., et al., *Gold nanocages as photothermal transducers for cancer treatment.* Small, 2010. **6**(7): p. 811-817.

30. Bickford, L., et al., *Enhanced multi-spectral imaging of live breast cancer cells using immunotargeted gold nanoshells and two-photon excitation microscopy.* Nanotechnology, 2008. **19**(31): p. 315102.

31. Barbosa, S., et al., *Tuning size and sensing properties in colloidal gold nanostars.* Langmuir, 2010. **26**(18): p. 14943-14950.

32. Minati, L., et al., *One-step synthesis of star-shaped gold nanoparticles.* Colloids and Surfaces A: Physicochemical and Engineering Aspects, 2014. **441**: p. 623-628.

33. Kumari, S. and R.P. Singh, *Glycolic acid-g-chitosan-gold nanoflower nanocomposite scaffolds for drug delivery and tissue engineering.* International journal of biological macromolecules, 2012. **50**(3): p. 878-883.

34. Chen, W., et al., *Structural-Engineering Rationales of Gold Nanoparticles for Cancer Theranostics.* Advanced Materials, 2016. **28**(39): p. 8567-8585.

35. Wang, H., et al., *Plasmonic nanostructures: artificial molecules.* Accounts of chemical research, 2007. **40**(1): p. 53-62.

36. Huang, P., et al., *Biodegradable gold nanovesicles with an ultrastrong plasmonic coupling effect for photoacoustic imaging and photothermal therapy.* Angewandte Chemie, 2013. **125**(52): p. 14208-14214.

37. Xia, Y., et al., *Gold nanocages: from synthesis to theranostic applications.* Accounts of chemical research, 2011. **44**(10): p. 914-924.

38. Millstone, J.E., G.S. Métraux, and C.A. Mirkin, *Controlling the edge length of gold nanoprisms via a seed-mediated approach.* Advanced Functional Materials, 2006. **16**(9): p. 1209-1214.

39. Zhang, Z., et al., *Mesoporous silica-coated gold nanorods as a light-mediated multifunctional theranostic platform for cancer treatment.* Advanced Materials, 2012. **24**(11): p. 1418-1423.

40. Wang, L., et al., *Novel insights into combating cancer chemotherapy resistance using a plasmonic nanocarrier: enhancing drug sensitiveness and accumulation simultaneously with localized mild photothermal stimulus of femtosecond pulsed laser.* Advanced Functional Materials, 2014. **24**(27): p. 4229-4239.

41. Ye, E., et al., *Plasmonic gold nanocrosses with multidirectional excitation and strong photothermal effect.* Journal of the American Chemical Society, 2011. **133**(22): p. 8506-8509.

42. Jiang, W., et al., *Nanoparticle-mediated cellular response is size-dependent.* Nature nanotechnology, 2008. **3**(3): p. 145-150.

43. Kong, L., et al., *RGD peptide-modified dendrimer-entrapped gold nanoparticles enable highly efficient and specific gene delivery to stem cells.* ACS applied materials & interfaces, 2015. **7**(8): p. 4833-4843.

44. Scarì, G., et al., *Gold nanoparticles capped by a GC-containing peptide functionalized with an RGD motif for integrin targeting.* Bioconjugate chemistry, 2012. **23**(3): p. 340-349.

45. Yin, H.-Q., et al., *One-step synthesis of linear and cyclic RGD conjugated gold nanoparticles for tumour targeting and imaging.* RSC Advances, 2014. **4**(18): p. 9078-9085.

46. Iyer, A.K., et al., *Exploiting the enhanced permeability and retention effect for tumor targeting.* Drug discovery today, 2006. **11**(17): p. 812-818.

47. Giljohann, D.A., et al., *Oligonucleotide loading determines cellular uptake of DNA-modified gold nanoparticles.* Nano letters, 2007. **7**(12): p. 3818-3821.

48. Dykman, L.A. and N.G. Khlebtsov, *Uptake of engineered gold nanoparticles into mammalian cells.* Chemical reviews, 2013. **114**(2): p. 1258-1288.

49. Kang, B., M.A. Mackey, and M.A. El-Sayed, *Nuclear targeting of gold nanoparticles in cancer cells induces DNA damage, causing cytokinesis arrest and apoptosis.* Journal of the American Chemical Society, 2010. **132**(5): p. 1517-1519.

50. Mukherjee, P., et al., *Potential therapeutic application of gold nanoparticles in B-chronic lymphocytic leukemia (BCLL): enhancing apoptosis.* Journal of nanobiotechnology, 2007. **5**(1): p. 4.

51. Ding, Y., et al., *Gold nanoparticles for nucleic acid delivery.* Molecular Therapy, 2014. **22**(6): p. 1075-1083.

52. Mirkin, C.A., et al., *A DNA-based method for rationally assembling nanoparticles into macroscopic materials.* Nature, 1996. **382**(6592): p. 607.

53. Rosi, N.L., et al., *Oligonucleotide-modified gold nanoparticles for intracellular gene regulation.* Science, 2006. **312**(5776): p. 1027-1030.

54. Cutler, J.I., E. Auyeung, and C.A. Mirkin, *Spherical nucleic acids.* Journal of the American Chemical Society, 2012. **134**(3): p. 1376-1391.

55. Rosi, N.L. and C.A. Mirkin, *Nanostructures in biodiagnostics.* Chemical reviews, 2005. **105**(4): p. 1547-1562.

56. Love, J.C., et al., *Self-assembled monolayers of thiolates on metals as a form of nanotechnology.* Chemical reviews, 2005. **105**(4): p. 1103-1170.

57. Zheng, D., et al., *Aptamer nano-flares for molecular detection in living cells.* Nano letters, 2009. **9**(9): p. 3258-3261.

58. Giljohann, D.A., et al., *Gene regulation with polyvalent siRNA− nanoparticle conjugates.* Journal of the American Chemical Society, 2009. **131**(6): p. 2072-2073.

59. Hurst, S.J., A.K. Lytton-Jean, and C.A. Mirkin, *Maximizing DNA loading on a range of gold nanoparticle sizes.* Analytical chemistry, 2006. **78**(24): p. 8313-8318.

60. Hurst, S.J., H.D. Hill, and C.A. Mirkin, *"Three-Dimensional Hybridization" with Polyvalent DNA− Gold Nanoparticle Conjugates.* Journal of the American Chemical Society, 2008. **130**(36): p. 12192-12200.

61. Chen, N., et al., *Self-Assembly of Poly-Adenine-Tailed CpG Oligonucleotide-Gold Nanoparticle Nanoconjugates with Immunostimulatory Activity.* Small, 2014. **10**(2): p. 368-375.

62. Massich, M.D., et al., *Cellular Response of Polyvalent Oligonucleotide− Gold Nanoparticle Conjugates.* ACS nano, 2010. **4**(10): p. 5641-5646.

63. Platt, N. and S. Gordon, *Is the class A macrophage scavenger receptor (SR-A) multifunctional?—The mouse's tale.* The Journal of clinical investigation, 2001. **108**(5): p. 649-654.

64. Chinen, A.B., C.M. Guan, and C.A. Mirkin, *Spherical Nucleic Acid Nanoparticle Conjugates Enhance G-Quadruplex Formation and Increase Serum Protein Interactions.* Angewandte Chemie International Edition, 2015. **54**(2): p. 527-531.

65. Storm, G., et al., *Surface modification of nanoparticles to oppose uptake by the mononuclear phagocyte system.* Advanced drug delivery reviews, 1995. **17**(1): p. 31-48.

66. Walkey, C.D. and W.C. Chan, *Understanding and controlling the interaction of nanomaterials with proteins in a physiological environment.* Chemical Society Reviews, 2012. **41**(7): p. 2780-2799.

67. Watson, J.D. and F.H. Crick, *A structure for deoxyribose nucleic acid.* Nature, 1953. **171**(4356): p. 737-738.

68. Kjems, J., E. Ferapontova, and K.V. Gothelf, *Nucleic acid nanotechnology*. 2014: Springer.

69. Williamson, J.R., M. Raghuraman, and T.R. Cech, *Monovalent cation-induced structure of telomeric DNA: the G-quartet model.* Cell, 1989. **59**(5): p. 871-880.

70. Gehring, K., J.-L. Leroy, and M. GuÃ, *A tetrameric DNA structure with protonated cytosine. cytosine base pairs.* Nature, 1993. **363**(6429): p. 561.

71. Cooper, G.M. and R.E. Hausman, *The cell*. 2000: Sinauer Associates Sunderland.

72. Baumketner, A., A. Jewett, and J. Shea, *Effects of confinement in chaperonin assisted protein folding: rate enhancement by decreasing the roughness of the folding energy landscape.* Journal of molecular biology, 2003. **332**(3): p. 701-713.

73. Vlassov, V.V., L.A. Blakireva, and L.A. Yakubov, *Transport of oligonucleotides across natural and model membranes.* Biochimica et Biophysica Acta (BBA)-Reviews on Biomembranes, 1994. **1197**(2): p. 95-108.

74. Bates, P.J., et al., *G-quadruplex oligonucleotide AS1411 as a cancer-targeting agent: Uses and mechanisms.* Biochimica et Biophysica Acta (BBA)-General Subjects, 2016.

75. Doherty, G.J. and H.T. McMahon, *Mechanisms of endocytosis.* Annual review of biochemistry, 2009. **78**: p. 857-902.

76. Miller, D.M., P.J. Bates, and J.O. Trent, *Antiproliferative activity of G-rich oligonucleotides and method of using same to bind to nucleolin*. 2008, Google Patents.

77. Đapić, V., et al., *Antiproliferative activity of G-quartet-forming oligonucleotides with backbone and sugar modifications.* Biochemistry, 2002. **41**(11): p. 3676-3685.

78. Schwartz, T.R., et al., *G-rich oligonucleotides alter cell cycle progression and induce apoptosis specifically in OE19 esophageal tumor cells.* Oligonucleotides, 2008. **18**(1): p. 51-63.

79. Qi, H., et al., *G-quadruplexes induce apoptosis in tumor cells.* Cancer research, 2006. **66**(24): p. 11808-11816.

80. Bates, P.J., E.W. Choi, and L.V. Nayak, *G-rich oligonucleotides for cancer treatment.* Gene Therapy of Cancer: Methods and Protocols, 2009: p. 379-392.

81. Rockwell, P., et al., *Cell-surface perturbations of the epidermal growth factor and vascular endothelial growth factor receptors by phosphorothioate oligodeoxynucleotides.* Proceedings of the National Academy of Sciences, 1997. **94**(12): p. 6523-6528.

82. Hartmann, G., et al., *Oligodeoxynucleotides enhance lipopolysaccharide-stimulated synthesis of tumor necrosis factor: dependence on phosphorothioate modification and reversal by heparin.* Molecular Medicine, 1996. **2**(4): p. 429.

83. Scaggiante, B., et al., *Human cancer cell lines growth inhibition by GTn oligodeoxyribonucleotides recognizing single-stranded DNA-binding proteins.* European Journal of Biochemistry, 1998. **252**(2): p. 207-215.

84. Burgess, T.L., et al., *The antiproliferative activity of c-myb and c-myc antisense oligonucleotides in smooth muscle cells is caused by a nonantisense mechanism.* Proceedings of the National Academy of Sciences, 1995. **92**(9): p. 4051-4055.

85. Gellert, M., M.N. Lipsett, and D.R. Davies, *Helix formation by guanylic acid.* Proceedings of the National Academy of Sciences, 1962. **48**(12): p. 2013-2018.

86. Huppert, J.L. and S. Balasubramanian, *Prevalence of quadruplexes in the human genome.* Nucleic acids research, 2005. **33**(9): p. 2908-2916.

87. Todd, A.K., M. Johnston, and S. Neidle, *Highly prevalent putative quadruplex sequence motifs in human DNA.* Nucleic acids research, 2005. **33**(9): p. 2901-2907.

88. Cheung, I., et al., *Disruption of dog-1 in Caenorhabditis elegans triggers deletions upstream of guanine-rich DNA.* Nature genetics, 2002. **31**(4): p. 405-409.

89. Zhao, Y., N.J. O'Neil, and A.M. Rose, *Poly-G/poly-C tracts in the genomes of Caenorhabditis.* BMC genomics, 2007. **8**(1): p. 403.

90. Sundquist, W.I. and A. Klug, *Telomeric DNA dimerizes by formation of guanine tetrads between hairpin loops.* 1989.

91. Duquette, M.L., et al., *Intracellular transcription of G-rich DNAs induces formation of G-loops, novel structures containing G4 DNA.* Genes & development, 2004. **18**(13): p. 1618-1629.

92. Balasubramanian, S., L.H. Hurley, and S. Neidle, *Targeting G-quadruplexes in gene promoters: a novel anticancer strategy?* Nature reviews Drug discovery, 2011. **10**(4): p. 261-275.

93. Patel, D.J., A.T. Phan, and V. Kuryavyi, *Human telomere, oncogenic promoter and 5'-UTR G-quadruplexes: diverse higher order DNA and RNA targets for cancer therapeutics.* Nucleic acids research, 2007. **35**(22): p. 7429-7455.

94. Collie, G.W. and G.N. Parkinson, *The application of DNA and RNA G-quadruplexes to therapeutic medicines.* Chemical Society Reviews, 2011. **40**(12): p. 5867-5892.

95. Sen, D. and W. Gilbert, *Formation of parallel four-stranded complexes by guanine-rich motifs in DNA and its implications for meiosis.* Nature, 1988. **334**(6180): p. 364-366.

96. Neidle, S. and S. Balasubramanian, *Quadruplex nucleic acids*. Vol. 7. 2006: Royal Society of Chemistry.

97. Jing, N., et al., *Targeting Stat3 with G-quartet oligodeoxynucleotides in human cancer cells.* DNA and cell biology, 2003. **22**(11): p. 685-696.

98. Jing, N., et al., *G-quartet oligonucleotides: a new class of Stat3 inhibitors that suppresses growth of prostate and breast tumors through induction of apoptosis*. 2004, AACR.

99. Xu, X., et al., *Inhibition of DNA replication and induction of S phase cell cycle arrest by G-rich oligonucleotides.* Journal of Biological Chemistry, 2001. **276**(46): p. 43221-43230.

100. Choi, E.W., L.V. Nayak, and P.J. Bates, *Cancer-selective antiproliferative activity is a general property of some G-rich oligodeoxynucleotides.* Nucleic acids research, 2009: p. gkp1088.

101. Bates, P.J., et al., *Antiproliferative activity of G-rich oligonucleotides correlates with protein binding.* Journal of Biological Chemistry, 1999. **274**(37): p. 26369-26377.

102. Galzio, R., et al., *Glycosilated nucleolin as marker for human gliomas.* Journal of cellular biochemistry, 2012. **113**(2): p. 571-579.

103. Goldshmit, Y., et al., *Interfering with the interaction between ErbB1, nucleolin and Ras as a potential treatment for glioblastoma.* Oncotarget, 2014. **5**(18): p. 8602-8613.

104. Reyes-Reyes, E.M., Y. Teng, and P.J. Bates, *A new paradigm for aptamer therapeutic AS1411 action: uptake by macropinocytosis and its stimulation by a nucleolin-dependent mechanism.* Cancer research, 2010. **70**(21): p. 8617-8629.

105. Reyes-Reyes, E., et al., *Mechanistic studies of anticancer aptamer AS1411 reveal a novel role for nucleolin in regulating Rac1 activation.* Molecular oncology, 2015. **9**(7): p. 1392-1405.

106. Narayan, S.P., et al., *The Sequence-Specific Cellular Uptake of Spherical Nucleic Acid Nanoparticle Conjugates.* small, 2015. **11**(33): p. 4173-4182.

107. Cavalieri, F., et al., *Thin multilayer films and microcapsules containing DNA quadruplex motifs.* small, 2011. **7**(1): p. 101-111.

108. Sengar, A., B. Heddi, and A.T.n. Phan, *Formation of G-quadruplexes in poly-G sequences: structure of a propeller-type parallel-stranded G-quadruplex formed by a G15 stretch.* Biochemistry, 2014. **53**(49): p. 7718-7723.

109. Lubitz, I. and A. Kotlyar, *G4-DNA-coated gold nanoparticles: synthesis and assembly.* Bioconjugate chemistry, 2011. **22**(10): p. 2043-2047.

110. Davis, J.T., *G-quartets 40 years later: from 5'-GMP to molecular biology and supramolecular chemistry.* Angewandte Chemie International Edition, 2004. **43**(6): p. 668-698.

111. Ali-Osman, F., *Brain tumors*. 2005: Springer Science & Business Media.

112. Jessen, K.R. and W.D. Richardson, *Glial cell development: basic principles and clinical relevance*. Vol. 1. 2001: Oxford University Press, USA.

113. Louis, D.N., et al., *The 2016 World Health Organization classification of tumors of the central nervous system: a summary.* Acta neuropathologica, 2016. **131**(6): p. 803-820.

114. Fabel, K., et al., *Long-term stabilization in patients with malignant glioma after treatment with liposomal doxorubicin.* Cancer, 2001. **92**(7): p. 1936-1942.

115. Avgeropoulos, N.G. and T.T. Batchelor, *New treatment strategies for malignant gliomas.* The Oncologist, 1999. **4**(3): p. 209-224.

116. Verkhratsky, A. and A.M. Butt, *Glial neurobiology*. 2007: John Wiley & Sons.

117. Runge, M.S. and C. Patterson, *Principles of molecular medicine*. 2007: Springer Science & Business Media.

118. Yaşargil, M.G. and C.D. Abernathey, *Microneurosurgery*. 1996: Thieme.

119. Fine, H.A., *The basis for current treatment recommendations for malignant gliomas.* Journal of neuro-oncology, 1994. **20**(2): p. 111-120.

120. Sharma, H.W., et al., *Differentiation of immortal cells inhibits telomerase activity.* Proceedings of the National Academy of Sciences, 1995. **92**(26): p. 12343-12346.

121. Kim, N.W., et al., *Specific association of human telomerase activity with immortal cells and cancer.* Science, 1994: p. 2011-2015.

122. Vietor, M., et al., *On the significance of telomerase activity in human malignant glioma cells.* European journal of pharmacology, 2000. **407**(1): p. 27-37.

123. Simone, R., et al., *G-quadruplexes: Emerging roles in neurodegenerative diseases and the non-coding transcriptome.* FEBS letters, 2015. **589**(14): p. 1653-1668.

124. Chong, E.Y., et al., *Telomerase expression in gliomas including the nonastrocytic tumors.* Human pathology, 1998. **29**(6): p. 599-603.

125. Langford, L.A., et al., *Telomerase activity in human brain tumours.* The Lancet, 1995. **346**(8985): p. 1267-1268.

126. Le, S., et al., *Telomerase activity in human gliomas.* Neurosurgery, 1998. **42**(5): p. 1120-1124.

127. Kondo, Y., et al., *Association between telomerase activity and basic fibroblast growth factor up-regulation in retinoblastomas.* Anticancer research, 2000. **21**(6A): p. 3765-3772.

128. Shay, J. and S. Bacchetti, *A survey of telomerase activity in human cancer.* European journal of cancer, 1997. **33**(5): p. 787-791.

129. Hiyama, K., *Telomeres and telomerase in cancer*. 2009: Springer.

130. Hakin-Smith, V., et al., *Alternative lengthening of telomeres and survival in patients with glioblastoma multiforme.* The Lancet, 2003. **361**(9360): p. 836-838.

131. Newlands, E., et al., *Phase I trial of temozolomide (CCRG 81045: M&B 39831: NSC 362856).* British journal of cancer, 1992. **65**(2): p. 287.

132. Glaser, T., et al., *Targeted nanotechnology in glioblastoma multiforme.* Frontiers in Pharmacology, 2017. **8**.

133. Cuddapah, V.A., et al., *A neurocentric perspective on glioma invasion.* Nature Reviews Neuroscience, 2014. **15**(7): p. 455-465.

134. Kievit, F.M., et al., *Chlorotoxin labeled magnetic nanovectors for targeted gene delivery to glioma.* Acs Nano, 2010. **4**(8): p. 4587-4594.

135. Khawaja, A.M., *The legacy of nanotechnology: revolution and prospects in neurosurgery.* International Journal of Surgery, 2011. **9**(8): p. 608-614.

136. Chiarelli, P.A., et al., *Bionanotechnology and the future of glioma.* Surgical neurology international, 2015. **6**(Suppl 1): p. S45.

137. Vieira, D.B. and L.F. Gamarra, *Getting into the brain: liposome-based strategies for effective drug delivery across the blood–brain barrier.* International Journal of Nanomedicine, 2016. **11**: p. 5381.

138. Sonavane, G., K. Tomoda, and K. Makino, *Biodistribution of colloidal gold nanoparticles after intravenous administration: effect of particle size.* Colloids and Surfaces B: Biointerfaces, 2008. **66**(2): p. 274-280.

139. Joh, D.Y., et al., *Selective targeting of brain tumors with gold nanoparticle-induced radiosensitization.* PloS one, 2013. **8**(4): p. e62425.

140. Hainfeld, J.F., et al., *Gold nanoparticle imaging and radiotherapy of brain tumors in mice.* Nanomedicine, 2013. **8**(10): p. 1601-1609.

141. Etame, A.B., et al., *Enhanced delivery of gold nanoparticles with therapeutic potential into the brain using MRI-guided focused ultrasound.* Nanomedicine: Nanotechnology, Biology and Medicine, 2012. **8**(7): p. 1133-1142.

142. Prades, R., et al., *Delivery of gold nanoparticles to the brain by conjugation with a peptide that recognizes the transferrin receptor.* Biomaterials, 2012. **33**(29): p. 7194-7205.

143. Qiao, Y., et al., *Identifying G-quadruplex-binding ligands using DNA-functionalized gold nanoparticles.* Analyst, 2012. **137**(7): p. 1663-1668.

144. Trickler, W.J., et al., *Brain microvessel endothelial cells responses to gold nanoparticles: In vitro pro-inflammatory mediators and permeability.* Nanotoxicology, 2011. **5**(4): p. 479-492.

145. Olivier, J.-C., *Drug transport to brain with targeted nanoparticles.* NeuroRx, 2005. **2**(1): p. 108-119.

146. O'donoghue, J. and T. Wheldon, *Targeted radiotherapy using Auger electron emitters.* Physics in medicine and biology, 1996. **41**(10): p. 1973.

147. Letfullin, R.R., C.B. Iversen, and T.F. George, *Modeling nanophotothermal therapy: kinetics of thermal ablation of healthy and cancerous cell organelles and gold nanoparticles.* Nanomedicine: Nanotechnology, Biology and Medicine, 2011. **7**(2): p. 137-145.

148. Meyers, J.D., et al., *Nanoparticles for imaging and treating brain cancer.* Nanomedicine, 2013. **8**(1): p. 123-143.

149. Terentyuk, G.S., et al., *Cancer laser thermotherapy mediated by plasmonic nanoparticles.* Handbook of Photonics for Biomedical Science, 2010. **20102371**.

150. Kang, S., et al., *Mesenchymal stem cells aggregate and deliver gold nanoparticles to tumors for photothermal therapy.* ACS nano, 2015. **9**(10): p. 9678-9690.

151. Madsen, S.J., et al., *Macrophages as cell-based delivery systems for nanoshells in photothermal therapy.* Annals of biomedical engineering, 2012. **40**(2): p. 507-515.

152. Bobyk, L., et al., *Photoactivation of gold nanoparticles for glioma treatment.* Nanomedicine: Nanotechnology, Biology and Medicine, 2013. **9**(7): p. 1089-1097.

153. Ruan, S., et al., *Tumor microenvironment sensitive doxorubicin delivery and release to glioma using angiopep-2 decorated gold nanoparticles.* Biomaterials, 2015. **37**: p. 425-435.

154. Verma, J., et al., *Delivery and cytotoxicity of doxorubicin and temozolomide to primary glioblastoma cells using gold nanospheres and gold nanorods.* European Journal of Nanomedicine, 2016. **8**(1): p. 49-60.

155. Meyers, J.D., et al., *Peptide-Targeted Gold Nanoparticles for Photodynamic Therapy of Brain Cancer.* Particle & Particle Systems Characterization, 2015. **32**(4): p. 448-457.

156. Velasco-Aguirre, C., et al., *Peptides and proteins used to enhance gold nanoparticle delivery to the brain: preclinical approaches.* International journal of nanomedicine, 2015. **10**: p. 4919.

157. Gromnicova, R., et al., *Glucose-coated gold nanoparticles transfer across human brain endothelium and enter astrocytes in vitro.* PLoS One, 2013. **8**(12): p. 81043.

158. Jensen, S.A., et al., *Spherical nucleic acid nanoparticle conjugates as an RNAi-based therapy for glioblastoma.* Science translational medicine, 2013. **5**(209): p. 209ra152-209ra152.

159. Ruan, S., et al., *Ligand Mediated and Enzyme-Directed Precise Targeting and Retention for Enhanced Treatment of Glioblastoma.* ACS Applied Materials & Interfaces, 2017.

160. Ruan, S., et al., *Increased Gold Nanoparticle Retention in Brain Tumors by in Situ Enzyme-Induced Aggregation.* ACS nano, 2016. **10**(11): p. 10086-10098.

161. Frosina, G., *Nanoparticle-mediated drug delivery to high-grade gliomas.* Nanomedicine: Nanotechnology, Biology and Medicine, 2016. **12**(4): p. 1083-1093.

162. Jewell, C.M., et al., *Oligonucleotide Delivery by Cell-Penetrating "Striped" Nanoparticles.* Angewandte Chemie International Edition, 2011. **50**(51): p. 12312-12315.

163. Barnaby, S.N., et al., *Design Considerations for RNA Spherical Nucleic Acids (SNAs).* Bioconjugate Chemistry, 2016. **27**(9): p. 2124-2131.

164. Yue, J., et al., *Gold nanoparticle size and shape effects on cellular uptake and intracellular distribution of siRNA nanoconstructs.* Bioconjugate Chemistry, 2017.

165. Kouri, F.M., et al., *miR-182 integrates apoptosis, growth, and differentiation programs in glioblastoma.* Genes & development, 2015. **29**(7): p. 732-745.

166. Zheng, Y., et al., *Radiosensitization of DNA by gold nanoparticles irradiated with high-energy electrons.* Radiation research, 2008. **169**(1): p. 19-27.

167. Ritchie, C., et al., *Combination of the aptamer AS1411 with paclitaxel or Ara-C produces synergistic inhibition of cancer cell growth*. 2007, AACR.

168. Bates, P.J., et al., *Discovery and development of the G-rich oligonucleotide AS1411 as a novel treatment for cancer.* Experimental and molecular pathology, 2009. **86**(3): p. 151-164.

169. Dam, D.H.M., K.S. Culver, and T.W. Odom, *Grafting aptamers onto gold nanostars increases in vitro efficacy in a wide range of cancer cell types.* Molecular pharmaceutics, 2014. **11**(2): p. 580-587.

170. Liu, X., et al., *Extinction coefficient of gold nanoparticles with different sizes and different capping ligands.* Colloids and Surfaces B: Biointerfaces, 2007. **58**(1): p. 3-7.

171. Jain, P.K., et al., *Calculated absorption and scattering properties of gold nanoparticles of different size, shape, and composition: applications in biological imaging and biomedicine.* J. Phys. Chem. B, 2006. **110**(14): p. 7238-7248.

172. Mirkin, C.A., A.K. Lytton-Jean, and S.J. Hurst, *Maximizing Oligonucleotide Loading on Gold Nanoparticle*. 2007, Google Patents.

173. Prather, R., A. Boquest, and B. Day, *Cell cycle analysis of cultured porcine mammary cells.* Cloning, 1999. **1**(1): p. 17-24.

174. Cho, E.C., Y. Liu, and Y. Xia, *A simple spectroscopic method for differentiating cellular uptakes of gold nanospheres and nanorods from their mixtures.* Angewandte Chemie International Edition, 2010. **49**(11): p. 1976-1980.

175. Thanh, N.T.K. and Z. Rosenzweig, *Development of an aggregation-based immunoassay for anti-protein A using gold nanoparticles.* Analytical chemistry, 2002. **74**(7): p. 1624-1628.

176. Chithrani, D.B., et al., *Gold nanoparticles as radiation sensitizers in cancer therapy.* Radiation research, 2010. **173**(6): p. 719-728.

177. Namboothiry, M.A., et al., *Electrochromic properties of conducting polymer metal nanoparticles composites.* Synthetic Metals, 2007. **157**(13): p. 580-584.

178. Lim, Z.-Z.J., et al., *Gold nanoparticles in cancer therapy.* Acta Pharmacologica Sinica, 2011. **32**(8): p. 983-990.

179. Nicol, J.R., D. Dixon, and J.A. Coulter, *Gold nanoparticle surface functionalization: a necessary requirement in the development of novel nanotherapeutics.* Nanomedicine, 2015. **10**(8): p. 1315-1326.

180. Peer, D., et al., *Nanocarriers as an emerging platform for cancer therapy.* Nature nanotechnology, 2007. **2**(12): p. 751-760.

181. McIntosh, C.M., et al., *Inhibition of DNA transcription using cationic mixed monolayer protected gold clusters.* Journal of the American Chemical Society, 2001. **123**(31): p. 7626-7629.

182. Shi, L., et al., *New Insight Into the Size Tuning of Monodispersed Colloidal Gold Obtained by Citrate Method.* arXiv preprint arXiv:1611.00951, 2016.

183. Miki, Y., et al., *Nucleolin Acts as a Scavenger Receptor for Acetylated Low-Density Lipoprotein on Macrophages.* Biological and Pharmaceutical Bulletin, 2015. **38**(9): p. 1420-1424.

184. Miki, Y., et al., *Nucleolin is a receptor for maleylated-bovine serum albumin on macrophages.* Biological and Pharmaceutical Bulletin, 2015. **38**(1): p. 116-121.

185. Sader, M., J. Courty, and D. Destouches, *Nanoparticles Functionalized with Ligands of Cell Surface Nucleolin for Cancer Therapy and Diagnosis.* J Nanomed Nanotechnol, 2015. **6**(310): p. 2.

186. Liang, Z., et al., *A centrifugation-based method for preparation of gold nanoparticles and its application in biodetection.* International journal of molecular sciences, 2007. **8**(6): p. 526-532.

187. Xu, Z., et al., *Knocking down nucleolin expression in gliomas inhibits tumor growth and induces cell cycle arrest.* Journal of neuro-oncology, 2012. **108**(1): p. 59-67.